Check for updates

Arteriosclerosis, Thrombosis, and Vascular Biology

ORIGINAL RESEARCH

Gut Microbial Metabolite Imidazole Propionate Impairs Endothelial Cell Function and Promotes the Development of Atherosclerosis

Vanasa Nageswaran, Alba Carreras, Leander Reinshagen, Katharina R. Beck, Jakob Steinfeldt, Marcus Henricsson, Pegah Ramezani Rad, Lisa Peters, Elisabeth T. Strässler, Joseph Lim, Barbara Verhaar, Yvonne Döring, Christian Weber, Maximilian König, Elisabeth Steinhagen-Thiessen, Ilja Demuth, Nicolle Kränkel, David M. Leistner, Michael Potente, Max Nieuwdorp, Petra Knaus, Wolfgang M. Kuebler, Marc Ferrell, Ina Nemet, Stanley L. Hazen, Ulf Landmesser,* Fredrik Bäckhed,* Arash Haghikia*

BACKGROUND: The microbially produced amino acid–derived metabolite imidazole propionate (ImP) contributes to the pathogenesis of type 2 diabetes. However, the effects of ImP on endothelial cell (EC) physiology and its role in atherosclerotic coronary artery disease are unknown. Using both human and animal model studies, we investigated the potential contributory role of ImP in the development of atherosclerosis.

METHODS: Plasma levels of ImP were measured in patients undergoing elective cardiac angiography (n=831) by ultra-high performance liquid chromatography coupled to tandem mass spectrometry. Odds ratios and corresponding 95% CIs for coronary artery disease were calculated based on the ImP quartiles using both univariable and multivariable logistic regression models. The effects of ImP on functional properties of ECs were assessed using human aortic ECs. In a mouse model of carotid artery injury, the impact of ImP on vascular regeneration was examined. Additionally, atheroprone *Apoe*$^{-/-}$ mice fed a high-fat diet were treated with and without ImP (800 µg), and aortic atherosclerotic lesion area was evaluated after 12 weeks. Next-generation sequencing, Western blot analysis, small interfering RNA–based gene knockdown, and tamoxifen-inducible Cre-loxP experiments were performed to investigate ImP-mediated molecular mechanisms.

RESULTS: Plasma ImP levels in subjects undergoing cardiac evaluation were associated with increased risk of prevalent coronary artery disease. We found that ImP dose dependently impaired migratory and angiogenic properties of human ECs and promoted an increased inflammatory response. Long-term exposure to ImP compromised the repair potential of the endothelium after an arterial insult. In atheroprone *Apoe*$^{-/-}$ mice, ImP increased atherosclerotic lesion size. Mechanistically, ImP attenuated insulin receptor signaling by suppressing the PI3K (phosphoinositide 3-kinase)/AKT pathway leading to sustained activation of the FOXO1 (forkhead box protein O1) transcription factor. Genetic inactivation of endothelial FOXO1 signaling in ImP-treated mice enhanced the angiogenic activity and preserved the vascular repair capacity of ECs after carotid injury.

CONCLUSIONS: Our findings reveal a hitherto unknown role of the microbially produced histidine-derived metabolite ImP in endothelial dysfunction and atherosclerosis, suggesting that ImP metabolism is a potential therapeutic target in atherosclerotic cardiovascular disease.

Key Words: forkhead box protein O1 ■ forkhead transcription factors ■ RNA, small interfering ■ tamoxifen ■ vascular system injuries

ATVB
Arteriosclerosis, Thrombosis, and Vascular Biology
FIRST PROOF ONLY

Correspondence to: Arash Haghikia, MD, Department of Cardiology, St. Josef University Hospital, Ruhr-University Bochum, Gudrunstraße 56, 44791 Bochum, Germany. Email arash.haghikia@ruhr-uni-bochum.de
*U. Landmesser, F. Bäckhed, and A. Haghikia contributed equally as senior authors.
Supplemental Material is available at https://www.ahajournals.org/doi/suppl/10.1161/ATVBAHA.124.322346.
For Sources of Funding and Disclosures, see page XXX.
© 2025 The Authors. *Arteriosclerosis, Thrombosis, and Vascular Biology* is published on behalf of the American Heart Association, Inc., by Wolters Kluwer Health, Inc. This is an open access article under the terms of the Creative Commons Attribution Non-Commercial-NoDerivs License, which permits use, distribution, and reproduction in any medium, provided that the original work is properly cited, the use is noncommercial, and no modifications or adaptations are made.
Arterioscler Thromb Vasc Biol is available at www.ahajournals.org/journal/atvb

Nonstandard Abbreviations and Acronyms

αSMA	α-smooth muscle actin
ACVD	atherosclerotic cardiovascular disease
CAD	coronary artery disease
DAPI	4′,6-diamidino-2-phenylindole
EC	endothelial cell
FOXO	forkhead box O transcription factor
HAEC	human aortic endothelial cell
ICAM-1	intercellular adhesion molecule-1
ImP	imidazole propionate
LDL	low-density lipoprotein
LPHN2	latrophilin 2
LRG1	leucine-rich-2-glycoprotein 1
ORO	oil red O
PE	phenylephrine
PFA	paraformaldehyde
PI3K	phosphoinositide 3-kinase
PI3K-C2A	phosphoinositide 3-kinase class IIα
TNF-α	tumor necrosis factor-α
UrdA	urocanate reductase
VCAM-1	vascular cell adhesion molecule-1
VLDL	very-low-density lipoprotein

Highlights

- Circulatory imidazole propionate (ImP) levels are higher in patients with atherosclerotic coronary artery disease than in patients without coronary artery disease.
- ImP attenuates vascular repair capacity after injury in mice.
- ImP promotes development of atherosclerosis in *Apoe*$^{-/-}$ mice.
- ImP impairs insulin receptor signaling in endothelial cells by suppressing the PI3K (phosphoinositide 3-kinase)/AKT pathway and subsequent activation of FOXO (forkhead box O transcription factor)-1 transcription factor.
- Targeting ImP-producing gut microbial pathways may provide a novel concept in cardiovascular disease prevention.

Endothelial cell (EC) dysfunction in the arterial vascular tree is the earliest detectable change in the development of atherosclerosis.[1] Impaired EC function compromises not only the ability to recover arterial integrity after injury but also promotes the adoption of a proinflammatory phenotype that attracts monocytes.[2] In patients with diabetes, EC dysfunction substantially increases the risk of atherosclerosis development. Targeting endothelial dysfunction is thus an important strategy for atherosclerotic cardiovascular disease (ACVD) prevention.[3]

In recent years, functional alterations of the gut microbiome and its metabolic activity have been increasingly acknowledged as causal factors of insulin resistance[4] and ACVD.[5] One such example of the causal contribution of metaorganismal pathways to ACVD is the metabolite trimethylamine *N*-oxide, which is derived from microbial metabolism of trimethylamine-containing nutrients such as choline and carnitine.[6] As shown in several animal models, trimethylamine *N*-oxide promotes the development of atherosclerosis and increases vascular thrombogenicity and atherothrombosis[5–9] with prognostic and clinical implications for patients with atherosclerotic coronary artery disease (CAD)[10–12] and ischemic stroke.[12]

Metagenomic approaches have linked specific gut microbiota composition with type 2 diabetes, as characterized by a decrease in the abundance of butyrate-producing bacteria and an increase in distinct potential opportunistic pathogens.[13–15] This altered ecosystem is associated with alterations in microbial metabolism and metabolite production.[16] Imidazole propionate (ImP), a histidine-derived metabolite, is increased in portal and peripheral blood of patients with type 2 diabetes compared with normoglycemic controls.[17,18] Importantly, when administered to mice, ImP caused glucose control impairment[17] and attenuated the glucose-lowering effect of metformin,[19] demonstrating a causal role for circulatory ImP in the pathogenesis of type 2 diabetes. Furthermore, ImP independently correlates with reduced ejection fraction and heart failure in clinical cohorts.[20] However, to date, the effect of ImP on EC function and its role in ACVD is unknown.

In this study, we sought to determine the association between circulatory ImP levels and CAD risk in humans. We investigated the effect of increased blood levels of ImP on EC function and how elevated ImP levels impact endothelial repair capacity after vascular injury in a mouse model. Furthermore, we explored the role of ImP in the development of atherosclerotic lesions in an *Apoe*$^{-/-}$ mice.

ATVB Arteriosclerosis, Thrombosis, and Vascular Biology FIRST PROOF ONLY

MATERIALS AND METHODS

Data Availability

RNA-sequencing data were made publicly available in the European Nucleotide Archive under accession number PRJEB61803 (https://www.ebi.ac.uk/ena/browser/view/PRJEB61803).

Material Availability

All data, analytic methods, and study materials are available to other researchers for purposes of reproducing these results or replicating these procedures by reasonable request directed to the corresponding author.[21] Detailed materials have been

incorporated in the article and are listed in the Major Resources Table in the Supplemental Material.

Human Studies

Blood samples were obtained from subjects enrolled in the LipidCardio study (German Clinical Trial Register; URL: drks.de; Unique identifier: DRKS00020915). The study was approved by the local research ethics committee (approval number: EA1/135/16), and all participants provided written informed consent. Study protocol and design of the LipidCardio study were described previously.[21]

Patients aged ≥18 years undergoing cardiac catheterization at a single large academic center (Deutsches Herzzentrum der Charité, Campus Benjamin Franklin), except those with troponin-positive acute coronary syndromes, were eligible for inclusion. Cardiac catheterization and coronary angiography were performed according to the standard protocols of the interventional cardiology unit and by discretion of the interventional cardiologist. The interventional cardiologist routinely documented diagnostic findings. Comprehensive angiographic results at the time of enrollment were recorded in the study database.

Blood samples were collected and processed to plasma before being frozen for storage. Between October 2016 and March 2018, 1005 consecutive patients were enrolled, from whom 831 blood samples were available for the current study. Comorbidities and cardiovascular risk factors, including diabetes, arterial hypertension, and dyslipidemia, were evaluated.

Patient samples and clinical data used for correlating ImP levels with soluble VCAM-1 (vascular cell adhesion molecule-1) levels were obtained from the GeneBank study conducted at the Cleveland Clinic: Molecular Determinants of Coronary Artery Disease (URL: https://www.clinicaltrials.gov; Unique identifier: NCT00590200). GeneBank is a single-site sample repository generated from consecutive patients undergoing elective diagnostic coronary angiography or elective cardiac computed tomographic angiography with extensive clinical and laboratory characterization and longitudinal follow-up. Subjects were recruited between 2001 and 2007. Exclusion criteria for GeneBank included patients with a recent myocardial infarction (<4 weeks) or elevated troponin I (>0.03 mg/dL) at enrollment. Subjects with atherosclerotic CAD were defined as patients with adjudicated diagnoses of stable or unstable angina, myocardial infarction, history of coronary revascularization, or angiographic evidence of ≥50% stenosis of at least 1 major coronary artery at the time of coronary angiography. All clinical study protocols and informed consent for human individuals were approved by the Cleveland Clinic Institutional Review Board. Written informed consent was obtained from all individuals. Soluble VCAM-1 levels were measured by ELISA according to the manufacturer's protocol (Invitrogen, Waltham, MA).

Blood Tests and ImP Measurement

Laboratory workup was performed for total cholesterol, LDLs (low-density lipoproteins), triglyceride, creatinine, and full blood count. Blood samples were immediately processed to plasma and stored in Central Biomaterial Bank Charité (ZeBanC) at −80 °C until the time of analysis. Plasma levels of ImP were quantified using ultra-high performance liquid chromatography coupled to tandem mass spectrometry. Analyses were performed in 2 different laboratories: the LipidCardio cohort was measured at Sahlgrenska University Hospital, University of Gothenburg, Sweden, and the GeneBank samples were assessed at the Cleveland Clinic. Both laboratories used the same internal standard (ImP-$^{13}C_3$) for their sample preparations. Samples from the European cohort were prepared and analyzed based on a previously published method with minor modifications.[17] Briefly, 25 µL of plasma samples were extracted using 6 volumes of acetonitrile containing 100 nmol/L of internal standard (ImP-$^{13}C_3$, Astra Zeneca, Cambridge, United Kingdom) before drying the samples under a flow of nitrogen. Then, the samples were reconstituted with 5% HCl (37%) in 1-butanol, subjected to n-butyl ester derivatization, and finally reconstituted in 150 µL water:acetonitrile (9:1). ImP levels were determined using multiple reaction monitoring of the transitions 197/81 and 200/82 for the internal standard.

Samples from the GeneBank study were subjected to LC-MS/MS analysis on a chromatographic system consisting of 2 Shimadzu LC-30 AD pumps (Nexera X2), a CTO 20 AC oven operating at 30 °C, and a SIL-30 AC-MP autosampler in tandem with 8050 triple quadruple mass spectrometer (Shimadzu Scientific Instruments Inc, Columbia, MD). The limit of quantification with a signal-to-noise cutoff of 10:1 was 5 nmol/L. Values below the limit of quantification were reported as half the limit of quantification value. Three quality control samples were performed with each sample batch and interbatch variations, expressed as coefficient of variation, were <10%. For data analysis, the LabSolution software (v5.89; Shimadzu) was used. Investigators performing analyses were blinded to sample identity other than barcode label.

Animal Models

Male wild-type C57BL/6J and *Apoe*$^{-/-}$ mice were purchased from Charles River Laboratories (Germany). Endothelial-specific FOXO (forkhead box O transcription factor)-1 knockout mice (*Cdh5-CreERT2*$^{(+/-)}$/*FOXO1*$^{fl/fl}$) on C57BL/6J background and control littermates without Cre recombinase (*Cdh5-CreERT2*$^{(+/+)}$/*FOXO1*$^{fl/fl}$) were obtained through collaboration.[22] All mouse experiments were performed in our animal facility and were approved by the ethics committee on animal care and use in Berlin, Germany. Mice were maintained under 12-hour light cycle with access to food and water ad libitum.

Adult (19–20 weeks of age) male *Apoe*$^{-/-}$ mice were fed a high-fat diet (crude fat, 34%; cholesterol, 290 mg/kg; Ssniff, Germany; E15741) for 12 weeks. Simultaneously, ImP (800 µg/d; Santa Cruz) or drinking water (used as control) was provided through drinking water to *Apoe*$^{-/-}$ mice. All mice were euthanized after 12 weeks of treatment. Blood was collected by cardiac puncture, and organs (heart and aorta) were isolated and snap-frozen in liquid nitrogen or dry ice and stored at −80 °C for further analysis.

To investigate the effect of ImP on arterial injury, adult (10 weeks of age) male C57BL/6J mice were randomly assigned to either control group (n=6) or ImP group (n=6) for a total of 24 days (Figure 3A). Carotid artery injury in mice was performed as described.[23] Briefly, mice were first anesthetized via inhalation of 3% isoflurane in oxygen (1 L/min) and then kept at 1.5% isoflurane until the intervention was finalized. Body temperature was maintained using a heating pad kept at 37 °C, preventing hypothermia during the procedure. After shaving the left side of the neck, a small incision was made to expose the left carotid artery. Carotid injury was induced to left carotid

AHA American Heart Association. ATVB Arteriosclerosis, Thrombosis, and Vascular Biology FIRST PROOF ONLY

artery by an electric impulse of 2 W for 2 s over a length of 4 mm using bipolar microforceps (VIO 50 C; Erbe Elektromedizin GmbH). Three days after carotid injury, reendothelialization was assessed by injecting 50 µL of 5% Evans blue (Sigma) into the left heart ventricle 2 minutes before euthanasia. Left carotid artery was isolated, rinsed in PBS, and fixed on microscope slides. The Evans blue–stained denuded area was captured en face using a brightfield microscope (Axioskop 40; Zeiss), and the reendothelialization was calculated longitudinally as the ratio of blue-stained area to injured area and subtracted from 100% by using imaging software (ImageJ; National Institutes of Health).

To assess the regulatory role of FOXO1 on vascular regeneration in vivo, adult endothelial-specific FOXO1 knockout mice (13 weeks of age) were generated by crossing *loxP*-flanked FOXO1 mice (*FOXO1*$^{fl/fl}$) with transgenic mice expressing the tamoxifen-inducible vascular endothelial-specific cadherin (*Cdh5*) promoter-driven CreERT2 recombinase.[22,24] Specifically, FOXO1 deletion (*Cdh5-CreERT2*$^{(+/-)}$/*FOXO1*$^{fl/fl}$; n=7) was induced by intraperitoneal injections of tamoxifen (100 mg per kg body weight; Sigma) dissolved in peanut oil (Sigma) and administered once daily for a total of 5 consecutive days. Littermate animals homozygous for the floxed *FOXO1*$^{fl/fl}$ but lacking the expression of Cre recombinase were used as a control group (*Cdh5-CreERT2*$^{(+/+)}$/*FOXO1*$^{fl/fl}$; n=6). After tamoxifen induction, animals were treated with ImP in drinking water for a total of 3 weeks before carotid artery injury.

Wire Myography

Isolated murine aortic segments of the ascending and descending aorta were mounted ex vivo into the chambers of a wire myograph (Multi Wire Myograph System 620M; Danish Myo Technology A/S) connected to PowerLab 4/35 (PL3504; ADInstruments) and the software LabChart 8 (ADInstruments). Following a 20-minute equilibration of the aortic tissue in physiological salt solution buffer, the vessels were stretched until a tension of 2 mN/3.5 mN for the ascending/descending aorta was achieved. Subsequently, a normalization protocol was conducted in accordance with the manufacturer's instructions. The maximum contraction was assessed by incubating the vessel segments in high potassium physiological salt solution buffer for 15 minutes. Following a period of washing, contraction against 50 nmol/L phenylephrine (PE; Sigma-Aldrich) in physiological salt solution was measured for 10 minutes. Subsequently, acetylcholine (Sigma-Aldrich) was added at 3-minute intervals in 8 increasing concentrations, covering a range from 10 nmol/L to 100 µmol/L. Subsequent to a 30-minute washing period utilizing physiological salt solution, 50 nmol/L PE was added into the solution once more. After 10 minutes, sodium nitroprusside (Sigma-Aldrich) was supplemented in a 3-minute cycle, spanning a concentration range of 100 pmol/L to 100 nmol/L. Dose-response curves were fitted to a sigmoidal curve using nonlinear regression. Data were normalized relative to the PE-induced maximal contraction and calculated as a percentage of the PE relaxation.

Lipid Analysis

Mouse plasma samples were subjected to fast-performance liquid chromatography (gel filtration on Superose 6 column; GE Healthcare). Different lipoprotein fractions were separated and evaluated based on flow-through time. Cholesterol levels were quantified using an enzymatic assay (c.f.a.s., Cobas; Roche Diagnostics) according to the manufacturer's protocol.

En Face Determination of Atherosclerosis

Atherosclerotic plaques were visualized using an en face method. Aortic arch and distributing branches were dissected from the mouse and opened longitudinally using a stereomicroscope (SMZ745T; Nikon). Aortas were fixed overnight with 4% paraformaldehyde (PFA), stained with oil red O (ORO; Sigma), and the aortic arch plaque area was calculated as the percentage of ORO-stained area to total aortic arch area.

Histology

For histological analysis of the aortic roots at the base of the heart (basis cordis), tissues were embedded in Tissue-Tek OCT (Sakura) and frozen at −80 °C until further processing. Tissues were cut into 6-µm-thick cryosections of the aortic root using a cryostat microtome (Microm HM 560; Thermo Fisher Scientific) and were fixed on glass slides (Super Frost Plus; Thermo Scientific). Before ORO staining, sections were fixed in 4% PFA for 10 minutes and washed twice in PBS for 5 minutes. Tissue sections were then incubated in 78% methanol for 5 minutes and stained for 10 minutes in fresh 0.5% ORO working solution dissolved in isopropanol. Following ORO staining, samples were rinsed in distilled water and nuclei were counterstained in hematoxylin (Carl Roth) before mounting in Kaiser glycerol gelatin (Merk). The percentage plaque area to total aortic root area was calculated using the ImageJ software.

Hematoxylin/eosin staining was used to assess aortic root morphology. Briefly, tissue sections were fixed in 10% formalin for 10 minutes, washed in PBS, and stained in Mayer hematoxylin for 15 s. After staining, sections were rinsed in tap water for 10 minutes and counterstained with eosin for 5 s. The sections were then dehydrated through graded ethanol and cleared in xylene, with each step repeated twice for 5 minutes. Images were taken using a Keyence fluorescence microscope.

Immunohistochemistry

Immunohistochemistry of frozen sections of the aortic roots was performed using the Avidin-Biotin Complex kits (Vector Laboratories). Briefly, acetone-fixed sections were washed in 1× PBS (without $Ca2^{+}$ and $Mg2^{+}$) before treatment with 0.075% H_2O_2 for 10 minutes to block endogenous peroxidase activity. The slides were then blocked with 10% rabbit serum (Dako) in Avidin-Biotin blocking solution (Vector Laboratories) for 30 minutes each. Sections were incubated with primary antibody against CD68 (Abcam; 1 µg/mL) for 1 hour and washed in PBS before being incubated with anti-rat biotinylated secondary antibody (Dako; 1:100) for 1 hour. The slides were then incubated with ABC-HRP Kit for Peroxidase (Vector Laboratories) for 30 minutes followed by 3-amino-9-ethylcarbazole (Sigma) staining for 12 minutes. Aortic roots were counterstained in hematoxylin solution (Carl Roth) for 15 s and washed in deionized water before mounting with Kaiser gelatin medium (Merk). Macrophage accumulation in plaque area was determined by calculating the percentage of CD68-positive staining to total aortic root area.

ATVB Arteriosclerosis, Thrombosis, and Vascular Biology FOR PROOF ONLY

FOXO1 En Face Immunostaining

After euthanizing the mice, vessels were perfused through the left ventricle with 10 mL of 1× PBS, followed by 2% PFA in PBS for 10 minutes. The aorta was then isolated and carefully cut open longitudinally to expose the endothelial surface. After fixation, the aorta was washed 3× in PBS for 10 minutes, permeabilized with 0.3% Triton X-100 in PBS for 15 minutes, and blocked with 10% donkey serum in PBS containing 0.1% Triton X-100 for 1 hour on an orbital shaker. Tissues were incubated with primary FOXO1 antibody (Cell Signaling; 1:100) in blocking buffer overnight at 4 °C in the dark. The following day, the aortas were washed, incubated with secondary antibody using DyLight-594–conjugated goat anti-rabbit IgG (H+L; Thermo Fisher; 2 µg/mL) for 1 hour, washed again 3×, and nuclei were counterstained with DAPI (4′,6-diamidino-2-phenylindole; 0.5 µg/mL in PBS) for 10 minutes. After the final rinse, tissues were mounted on a slide with a coverslip using fluorescent mounting medium (Dako) and imaged on the Leica TCS SPE-II confocal microscope at ×40 oil immersion magnification.

Cell Culture

Primary human aortic ECs (HAECs; Cell Applications) were used between passages 7 and 9 for experiments. HAECs were cultured in endothelial growth medium-2 (PromoCell GmbH) supplemented with 10% fetal bovine serum, 100 units/mL penicillin, and 100 µg/mL streptomycin. Human THP-1 monocytes were cultured in RPMI 1640 medium (Gibco) supplemented with 10% fetal bovine serum, 2 mmol/L L-glutamine, 100 U/mL penicillin, and 100 µg/mL streptomycin. Cells were grown to confluence at 37 °C and 5% CO_2 before experiments.

Wound Healing Assay

Endothelial wound healing potential was assessed by cell scratch assay in vitro. HAECs (6×10^4 per well) were seeded on fibronectin-coated 24-well culture plate overnight, and then serum-starved (0.5% fetal bovine serum) for 5 hours at 37 °C in cell culture incubator before stimulation. The cells were scratched using a sterile 100 µL yellow pipette tip and treated with 10 nmol/L ImP, 100 nmol/L ImP, 10 ng/mL recombinant TNF-α (tumor necrosis factor-α) or control for 16 hours. Pictures of the wound area were taken at times 0 and 16 hours post-migration using a phase-contrast microscope (EVOS XL Core; Thermo Fisher Scientific). The width of the scratch was measured and quantified by ImageJ software (v1.53s).

BrdU Cell Proliferation

ECs were seeded at a density of 5000 cells per well in a 96-well plate and allowed to adhere overnight in complete growth media. Cells were treated with or without 100 nmol/L ImP for 24 hours or with mitomycin C (10 µg/mL) for 5 hours as positive control for inhibition of cell proliferation. BrdU incorporation analysis was performed according to the manufacturer's protocol (Roche Diagnostics), and absorbance was measured at 450 nm using a microplate reader (Tecan).

Tube Formation Assay

To evaluate the effect of ImP on tube formation, 1.5×10^4 HAECs per well were cultured on Matrigel using growth factor–reduced basement membrane extract (Gibco) in 96-well flat bottom plate and stimulated in conditioned medium with control, 50 ng/mL IGF-1, 100 nmol/L ImP, or 10 ng/mL recombinant TNF-α for 16 hours. After tubular network was formed by HAECs, cells were stained with 6 µmol/L Calcein AM solution (R&D Systems) for 15 minutes at 37 °C. Representative images were taken using an inverted fluorescent microscope (BZ-X; Keyence Corporation), and tube formation was evaluated with Angiogenesis Analyzer tool in ImageJ software (v1.53s) by quantifying the total number of segments normalized to control.

Flow Cytometry of HAECs

Expression of cellular adhesion molecules of ICAM-1 (intercellular adhesion molecule-1), VCAM-1, and E-selectin was assessed by fluorescence-activated cell sorting. HAECs (6×10^4 per well) were seeded on 24-well plates and stimulated with control medium, 10 nmol/L ImP, or 100 nmol/L ImP for 24 hours before being washed and collected into fluorescence-activated cell sorting tubes (BD Biosciences). Cells were incubated with the following antibodies: CD54 (AF700, HA58, 1:100), CD106 (APC, STA, 1:100), and CD62E (PE/Cy7, HAE-1f, 1:100) for 15 minutes at room temperature. All antibodies were purchased from BioLegend. Fluorescence-minus controls and unstained HAECs were included in the measurements. Samples were acquired using Attune Nxt Flow Cytometer (Thermo Fisher Scientific), and cells were analyzed with Kaluza software (Beckman and Coulter).

Flow Adhesion Assay

Monocyte-EC interaction was investigated by a flow-based adhesion assay. HAECs were seeded in ibidi y-shaped chamber slides (ibidi GmbH) for 5 hours and then incubated overnight under sterile flow conditions using a shear stress of 20 dyn/cm^2. After acclimatization, cells were treated with control, 10 nmol/L ImP, or 100 nmol/L ImP for 24 hours, respectively. Finally, THP-1 monocytes (1×10^6 cells/mL) were labeled with Dil cell staining solution (Invitrogen) before being perfused through the chambers for 30 minutes. After incubation, nonadherent monocytes were removed with PBS, and cocultures were fixed with 4% PFA. The number of adherent monocytes to HAECs was quantified from different fields of view using a fluorescence phase-contrast microscope (BZ-X; Keyence Corporation).

Western Blotting

Whole-cell lysates from washed ECs were obtained using RIPA buffer (50 mmol/L Tris, 150 mmol/L NaCl, 1 mmol/L EDTA, 1 mmol/L NaF, 1 mmol/L DTT, 10 mg/mL aprotinin, 10 mg/mL leupeptin, 0.1 mmol/L Na_3VO_4, 1 mmol/L PMSF, and 0.5% NP-40, pH 7.5). Lysates were centrifuged for 10 minutes at 14 000 rpm and 4 °C followed by protein determination with Pierce BCA Protein Assay Kit (Thermo Scientific) according to the manufacturer's instructions. 20 µg of protein was separated by 10% SDS-PAGE and transferred onto a PVDF membrane (Merck). Membranes were blocked in 5% milk or BSA for 1 hour at room temperature and incubated with primary antibodies against PI3K-C2A (PI3K class IIα; Cell Signaling; 1:2000), phospho-AKT(Ser473; Cell Signaling; 1:1000), AKT (Cell

ATVB Arteriosclerosis, Thrombosis, and Vascular Biology PROOF ONLY

Signaling; 1:1000), phospho-FOXO1(Thr24; Cell Signaling; 1:2000), FOXO1 (Cell Signaling; 1:2000), and GAPDH (Merck; 0.02 µg/mL) overnight at 4 °C. Membranes were then incubated with horseradish peroxidase–conjugated anti-rabbit or anti-mouse secondary antibody (Southern Biotechnology) for 1 hour at room temperature. Membranes used to detect phospho-target proteins were stripped in a low-pH glycine buffer (1.5% glycine, 0.1% SDS, and 1% Tween-20, pH 2.2) for 20 minutes, reblocked, and reprobed with antibodies against the total target protein and loading control (GAPDH). Proteins were detected with SuperSignal West Dura Extended Duration Substrate (Thermo Scientific), and the intensity of chemiluminescence was measured using a UVP ChemStudio PLUS imaging system (Analytik Jena).

Immunocytochemistry

HAECs were grown on fibronectin-coated glass slides and treated with versus without ImP (100 nmol/L) for 24 hours. Cells were then washed and fixed with 4% PFA for 15 minutes at room temperature. Permeabilization was performed in 0.5% Triton X-100 in PBS for 15 minutes and blocking in 5% horse serum for 1 hour. HAECs were stained overnight for anti-FOXO1 (Cell Signaling; 1:100) and DAPI (Roche Diagnostics; 0.1 µg/mL) followed by DyLight-594–conjugated goat anti-rabbit secondary antibody (Invitrogen; 1:100) for 1 hour. Cells were washed and mounted in Kaiser glycerol gelatin (Merck). The fluorescence intensity of nuclear FOXO1 staining was analyzed with a Keyence fluorescence microscope.

Small Interfering RNA Transfection

HAECs were plated at a density of 3×10^5 cells per well in a 6-well format before being transfected with FOXO1 small interfering RNA or scramble small interfering RNA (ON-TARGETplus; Dharmacon) for 4 hours in Opti-MEM medium (Gibco) using Lipofectamine RNAiMAX transfection kit (Invitrogen) according to the manufacturer's protocol. *FOXO1* gene silencing efficacy was confirmed on protein levels by Western blot analysis.

RNA Sequencing

Total RNA was extracted from ECs after stimulation with ImP (100 nmol/L) or control for 12 hours using the RNeasy Mini Kit (Qiagen) according to the manufacturer's instructions. RNA purity and yield were assessed with NanoVue (GE Healthcare), and ribosomal RNA integrity was confirmed by agarose gel electrophoresis stained with ethidium bromide. Three replicates from 3 independent experiments were performed for next-generation sequencing. RNA library preparation, sequencing, and alignment of the reads was outsourced to GENEWIZ from Azenta Life Sciences (Leipzig, Germany). Library preparation was performed using the NEBNext Ultra II Directional RNA Library Prep Kit following the manufacturer's instructions (oligodT enrichment method). Samples were sequenced on the Illumina Novoseq 6000 platform with 150-bp paired-end reads. Sequences were trimmed to remove adapter sequences and nucleotides with poor quality using Trimmomatic (v0.36). The trimmed reads were mapped to the human genome reference ENSEMBL version 86 using the STAR aligner (v2.5.2b). Read counts were calculated with the featureCounts program in the Subread package (v1.5.2), only counting unique gene hits. The mean number of total reads per sample was 29.2±3.5 million, of which 99.6% were mapped, resulting in on average 25±3.8 million counts per sample.

Statistical Analysis

Statistical analyses for the in vitro and in vivo analyses were performed by GraphPad Prism 9 (GraphPad Software Inc; v9.3.1 to v10.1.0) and presented as mean±SEM. Normal distribution of data was assessed using the Shapiro-Wilk test and was analyzed by unpaired 2-tailed Student *t* test (for 2 groups) or 1-way ANOVA followed by Bonferroni post hoc test for multiple comparisons (for ≥3 groups). Data that passed the normality test but with unequal variance were assessed by the Welch *t* test or Brown-Forsythe and Welch ANOVA tests followed by Dunnett T3 post hoc test for multiple comparisons. Otherwise, nonparametric statistical analyses were performed using the Mann-Whitney *U* test for 2 groups or the Kruskal-Wallis test followed by the Dunn post hoc test for multiple comparisons (for ≥3 groups). Data in dose-contraction curves are expressed as a percentage of PE-induced vasoconstriction against the log molar concentration of vasodilators (acetylcholine and sodium nitroprusside) and were fitting to a sigmoidal curve using nonlinear regression. Overall differences in responses between the groups (control versus ImP) and across different concentrations were assessed using 2-way ANOVA, followed by Bonferroni post hoc analysis. Differential gene expression was performed using the DESeq2 package (v1.36.0) in RStudio (v2022.07.2+576) with R (v4.2.1)25. Read counts for control and ImP conditions were analyzed with a Wald test and parametric fit to identify differentially expressed genes. *P* values were adjusted using false discovery rate multiple testing correction. Genes with an adjusted $P<0.1$ were considered as differentially expressed between control and ImP. Read counts were normalized using DESeq2's median of ratios method to account for sequencing depth and RNA composition.[25] A volcano plot was drawn using ggplot2 (v3.4.0). After zero mean, unit variance scaling of the normalized read counts, a heatmap with differentially expressed genes was drawn using the ComplexHeatmap package (v2.12.1). The dendrogram in this plot was constructed with Ward method. The code for the differential gene expression analyses was shared in a Github repository (https://github.com/barbarahelena/transcriptomics-imp-charite).

In the human studies, odds ratios and corresponding 95% CIs for CAD were calculated based on the ImP quartiles using both univariable and multivariable logistic regression models. In the multivariable models, adjustments were made for age and sex only, as well as established cardiovascular risk factors including age, sex, smoking status, hypertension, hypercholesterolemia, and diabetes. Significance was assumed at a 2-sided *P* value of $P\leq0.05$.

RESULTS

Plasma Levels of ImP Are Associated With CAD

To investigate whether ImP is associated with CAD, we examined ImP plasma levels and CAD risk in a patient cohort (n=831) undergoing elective cardiac evaluation. Levels of ImP in individuals with CAD were significantly higher than in individuals without CAD.

ATVB Arteriosclerosis, Thrombosis, and Vascular Biology FIRST PROOF ONLY

Patient demographics, laboratory values, and clinical characteristics of all patients are provided in the Table. We also compared these parameters between patients with and without CAD. Plasma levels of ImP were increased in patients with significant (≥50% stenosis) angiographic evidence of CAD (Figure 1A), as revealed by diagnostic cardiac catheterization (Figure 1B) with a dose-dependent relationship between ImP levels and the prevalence of CAD (Figure 1C). This association was particularly pronounced in patients in the fourth quartile and remained significant after adjustments for both age and sex (model 1: odds ratio, 3.80 [95% CI, 2.39–6.15]; $P<0.05$) and even after further adjustments for cardiovascular risk factors including hypertension, dyslipidemia, diabetes, and smoking (model 2: odds ratio, 4.22 [95% CI, 2.60–6.97]; $P<0.05$). Notably, we found significantly higher levels of ImP in patients with diabetes than in controls (Figure S1), confirming previous findings demonstrating diabetogenic effects of ImP.[17]

ImP Impairs Migratory and Angiogenic Properties of ECs

Given the central role of endothelial dysfunction in atherosclerosis,[26] we hypothesized that elevated ImP levels may contribute to the pathogenesis of ACVD by compromising the properties of ECs. We thus treated HAECs with ImP to assess its impact on the migration, proliferation, and angiogenic properties of ECs. ImP significantly reduced gap closure in an in vitro scratch injury assay, suggesting an impaired EC migratory capacity (Figure 2A and 2B). Additionally, BrdU incorporation analysis revealed a significant decrease in EC proliferation rates in ImP-treated cells compared with untreated controls (Figure S2). To further address whether the reduced migratory and proliferative capacities resulted in defective angiogenic activity, we next used a Matrigel angiogenesis assay. We observed significantly reduced tube formation in ImP-pretreated ECs compared with control cells, indicating that ImP impairs angiogenic potential in ECs (Figure 2C and 2D). Together, these results suggest that ImP may impair EC functions, which are important for wound healing in the vessel wall.

Table. Baseline Clinical Parameters and Laboratory Test Results

Characteristic	Overall, N=831	CAD, n=577	No CAD, n=254	*P* value*
Age, y	75 (66, 81)	76 (67, 81)	72 (62, 79)	<0.001
Sex				<0.001
Female	248 (30%)	124 (21%)	124 (49%)	
Male	583 (70%)	453 (79%)	130 (51%)	
Imidazol propionate, nmol/L	12 (8, 24)	13 (8, 26)	10 (7, 18)	<0.001
Hypertension	668 (80%)	477 (83%)	191 (75%)	0.012
Hypercholesterinaemia	497 (60%)	378 (66%)	119 (47%)	<0.001
Diabetes	232 (28%)	178 (31%)	54 (21%)	0.005
Smoker	140 (17%)	98 (17%)	42 (17%)	0.90
Creatinine, mg/dL	0.97 (0.84, 1.16)	1.00 (0.84, 1.19)	0.92 (0.81, 1.05)	<0.001

Values are expressed as median (IQR) and n (%). CAD indicates coronary artery disease; and IQR, interquartile range.

*Wilcoxon rank-sum test; Pearson χ^2 test.

ImP Promotes Endothelial Inflammation by Inducing the Expression of Adhesion Molecules

We evaluated whether impaired EC functions were associated with proinflammatory activation, a hallmark feature that promotes atherogenesis. To this end, we performed fluorescence-activated cell sorting analyses to evaluate the expression of EC adhesion molecules on HAECs as markers of endothelial inflammation and observed a dose-dependent increase in the expression of ICAM-1, E-selectin, and VCAM-1; Figure 2E; Figure S3, gating strategy). The increased expression of adhesion molecules on ECs following ImP treatment translated to increased monocyte adhesion (Figure 2F and 2G). Since activated endothelium releases soluble VCAM-1 leading to increased circulatory soluble VCAM-1 levels in blood,[26] we also investigated the interaction between circulating soluble VCAM-1 and ImP levels in a second cohort (the GeneBank cohort) consisting of consecutive patients undergoing elective diagnostic coronary angiography or elective cardiac computed tomographic angiography. Soluble VCAM-1 significantly correlated with circulating ImP levels (Figure S4) further supporting proinflammatory actions of ImP leading to increased expression of adhesion molecules.

ImP Impairs Arterial Regeneration After Carotid Injury and Endothelium-Dependent Aortic Relaxation

In view of the observed detrimental effects of ImP on EC functions in vitro, we evaluated the systemic relevance of ImP-mediated effects on vascular regeneration using a mouse carotid artery injury model (Figure 3A). To this end, mice were subjected to ImP or control water via drinking water for 3 weeks before undergoing carotid artery injury. Three days after injury, vascular regeneration was evaluated by Evans blue staining, which determines the denuded area (blue stained). Our results show that treatment with ImP significantly impaired the wound healing process as compared with the control group (Figure 3B and 3C) and, thus, highlight the deleterious effects of ImP on vascular repair mechanisms in vivo.

ATVB Atherosclerosis, Thrombosis, and Vascular Biology FIRST PROOF ONLY

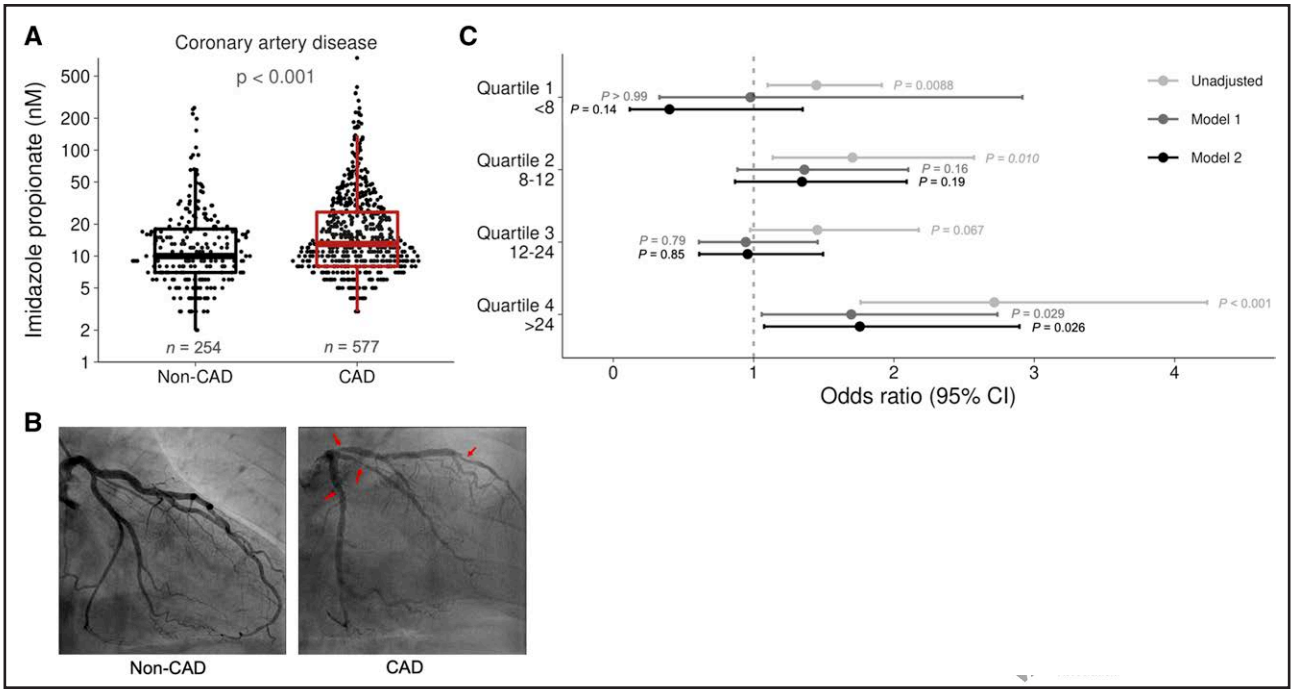

Figure 1. Increased imidazole propionate (ImP) plasma levels are associated with atherosclerotic cardiovascular disease. **A**, Box-whisker plots of circulating ImP levels in patients without coronary artery disease (CAD) as compared with patients with CAD. Data are represented as box plots: the middle line is the median, the lower and upper hinges are the first and third quartiles, and the whiskers represent the 10th and 90th percentiles. **B**, Coronary angiography from patients with different ImP levels. The representative images show a patient with low ImP levels within the first quartile without any atherosclerotic alterations in the coronary arteries (**left**) and a patient with high ImP levels within the fourth quartile (**right**), exhibiting multiple stenotic segments (red arrows). **C**, Odds of CAD among all test subjects according to ImP quartile levels using multivariable logistic regression models. Unadjusted odds ratio, adjusted model 1 (age and sex), and adjusted model 2 (model 1 plus incidence of hypertension, dyslipidemia, diabetes, and smoking). Symbols represent odds ratio, and the 95% CIs are indicated by the line length. Data are shown as mean±SEM and were calculated using the Wilcoxon rank-sum test (n=831).

ATVB Arteriosclerosis, Thrombosis and Vascular Biology FIRST PROOF ONLY

To assess whether ImP-induced vascular dysfunction is endothelium dependent, we performed wire myography of freshly isolated murine aorta ex vivo. ImP treatment significantly impaired endothelium-dependent vasorelaxation in response to acetylcholine in both the ascending and descending aortas compared with the control group. Notably, no significant difference was observed in the endothelium-independent relaxation response to sodium nitroprusside between both groups, further supporting that ImP specifically induces EC dysfunction in vivo (Figure 3D).

ImP Aggravates High-Fat Diet–Induced Atherosclerosis in *Apoe*$^{-/-}$ Mice

To investigate whether ImP could directly promote CAD, we assessed atherosclerosis development in *Apoe*$^{-/-}$ mice receiving ImP via drinking water for 12 weeks (Figure 4A). As expected, this protocol induced a 12-fold increase in plasma ImP levels (Figure 4B), which aligns with the upper range observed in patients with the highest levels of ImP. Treatment with ImP neither affected blood levels of total cholesterol, nor did it affect atheroprone VLDL (very-low-density lipoprotein) and LDL (low-density lipoprotein) cholesterol compared with the control group (Figure 4C and 4D). In contrast, chronic ImP administration increased atherosclerotic lesion size with enhanced vascular smooth muscle cell (αSMA [α-smooth muscle actin]) activation and increased accumulation of CD68^{+} macrophages in the atherosclerotic lesion area of *Apoe*$^{-/-}$ mice (Figure 4E and 4F), highlighting the proatherogenic and proinflammatory effects of ImP, independent of circulating lipoprotein levels. ImP treatment under standard laboratory diet showed no significant difference in plaque formation (Figure S5B and S5C).

ImP Suppresses PI3K/AKT Signaling and Promotes Activation of Nuclear FOXO1

To elucidate the underlying molecular mechanism, RNA sequencing of ImP-treated and untreated HAECs was performed. A total of 52 genes were differentially expressed between the ImP and control conditions, of which 18 genes were upregulated and 34 genes were downregulated in ImP-treated ECs compared with control (Figure 5A and 5B). Notably, several genes involved in angiogenesis were differentially expressed after ImP treatment, including *ADGRL2*, *CALCRL*, *FLT1*, *TM4SF18*, *DCHS1*, *FLRT2*, *ANGPTL4*, *ARGHGAP22*,

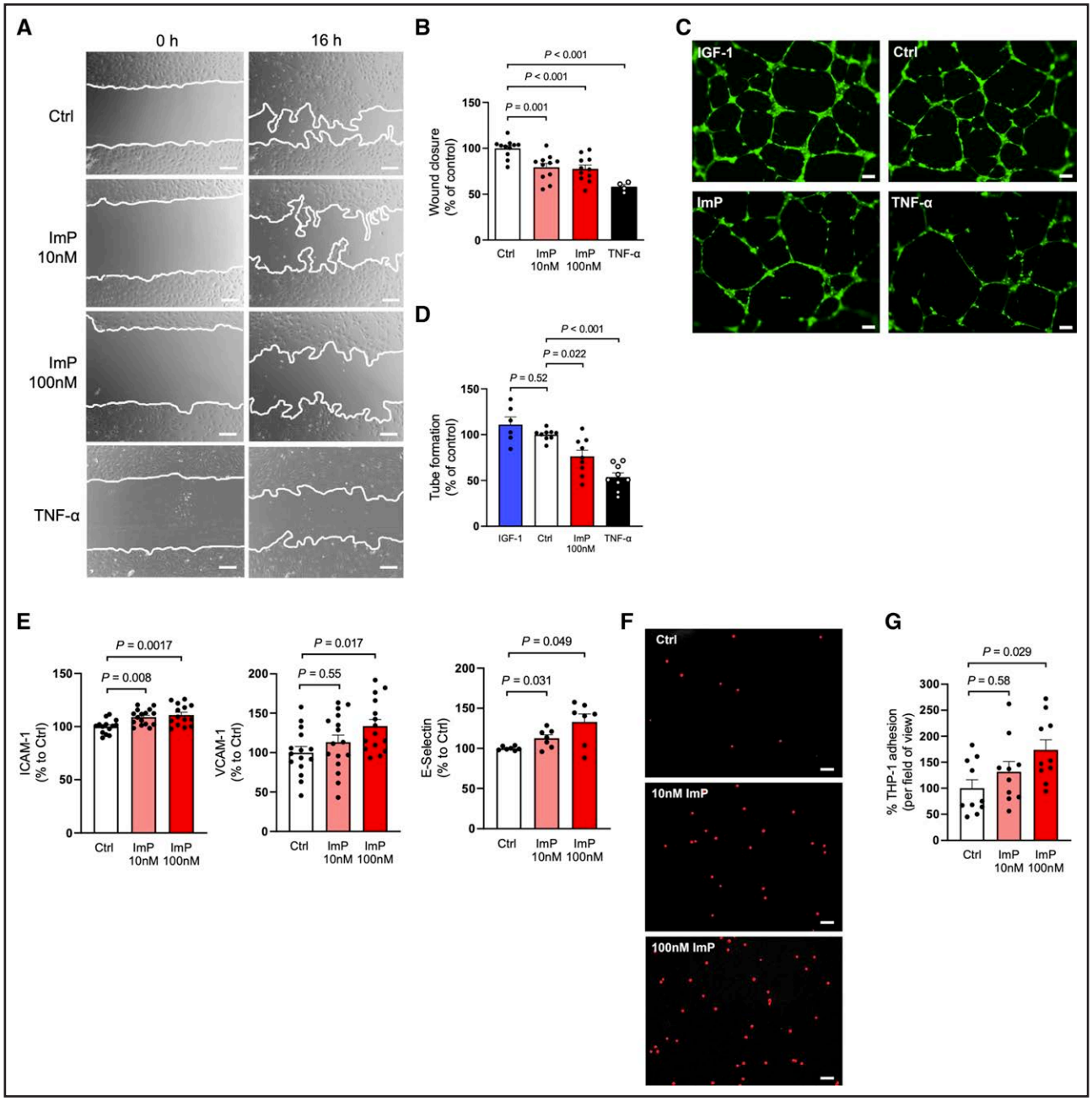

Figure 2. Imidazole propionate (ImP) impairs migratory and angiogenic properties, while also promoting inflammatory activation of endothelial cells.

A, Scratch wound healing assay. Representative migration images of human aortic endothelial cells (HAECs) treated with and without ImP or TNF-α (tumor necrosis factor-α) for 16 hours (×10 magnification; scale bars represent 200 μm). **B**, Quantification of migration capacity (n=4 for the TNF-α group and n=11 for all other groups). Comparison of wound healing area between control (Ctrl) and treatment with 10 nmol/L ImP, 100 nmol/L ImP, or 10 ng/mL TNF-α. **C**, Matrigel tube formation assay. Representative images of endothelial tube formation upon 16-hour treatment with IGF-1 (50 ng/mL), Ctrl, ImP (100 nmol/L), and TNF-α (10 ng/mL) were taken after Calcein AM staining (green; ×10 magnification; scale bars represent 100 μm). **D**, Endothelial tube formation was quantified by the total number of segments as percentages to control (n=6 for IGF-1 group and n=9 for all other groups). **E**, ImP increases the expression of proinflammatory cellular adhesion molecules ICAM-1 (intercellular adhesion molecule-1), VCAM-1 (vascular cell adhesion molecule-1), and E-selectin. Quantitative data are shown as the percentage of gated mean fluorescence intensity (MFI) to control (n=15 for ICAM-1 and VCAM-1 analysis; n=7 for E-selectin analysis). **F**, Representative images of DiI-labeled THP-1 monocytes (red dots) adhered to endothelial cells upon 24-hour stimulation with 10 and 100 nmol/L ImP (×10 magnification; scale bars represent 100 μm). **G**, Quantification of THP-1 monocyte adhesion to HAECs per field of view in percentage (n=10 per group). Data are shown as mean±SEM and were calculated by 1-way ANOVA followed by the Bonferroni post hoc analysis for multiple comparisons (**B**, **D**, and **E**) or by Kruskal-Wallis test followed by the Dunn post hoc analysis for multiple comparisons (**G**). Data with unequal variances (**D** and **E**, E-selectin) were assessed by Welch ANOVA test with Dunnett T3 post hoc test for multiple comparisons.

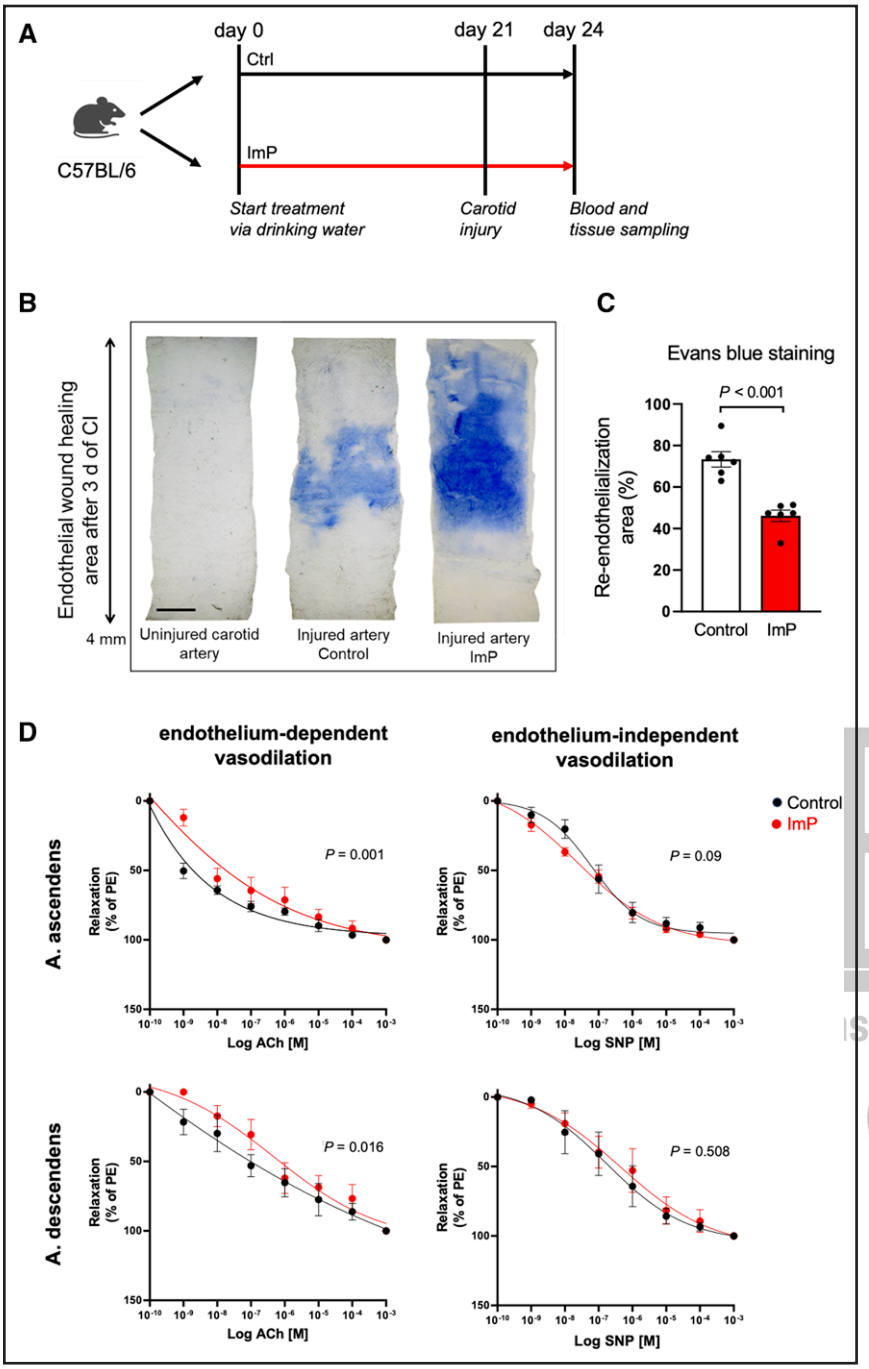

Figure 3. Imidazole propionate (ImP) impairs arterial regeneration after carotid injury (CI) and induces endothelial dysfunction in vivo. **A**, Schematic illustration of the experimental setup for the murine CI model. Control (Ctrl) or ImP was provided to adult C57BL/6J mice in drinking water for a total of 24 days. At day 21, CI was induced to the left carotid artery, and vascular reendothelialization was analyzed after a healing period of 3 days by Evans blue staining. **B**, Representative en face images of Evans blue–stained carotid arteries: uninjured carotid artery, injured carotid artery of the Ctrl and ImP groups. The blue-stained area corresponds to the denuded area of injured carotid arteries (×5 magnification; scale bar represents 500 μm). **C**, Quantification of reendothelialization as the ratio of blue-stained area to total injured area in percentage. Data are shown as mean±SEM and were calculated by unpaired 2-tailed Student *t* test between the Ctrl and ImP groups (n=6 per group). **D**, Vascular reactivity and functional response of murine aortic segments of the ascending and descending aortas were assessed by ex vivo wire myography upon treatment of ImP or Ctrl condition (n=6). Endothelium-dependent relaxation was measured on phenylephrine (PE)-contracted (50 nmol/L) aortic rings followed by cumulative dose-response curves to acetylcholine (ACh; 10 nmol/L to 100 μmol/L). Endothelium-independent aortic relaxation was noted with sodium nitroprusside (SNP; 100 pmol/L to 100 nmol/L) during contraction with PE (50 nmol/L). Dose-response curves were fitted to a sigmoidal curve using nonlinear regression. Maximal contraction response was calculated as a percentage of the PE. Data are shown as mean±SEM and were assessed for overall differences in responses between the groups (Ctrl vs ImP) and across different concentrations using 2-way ANOVA followed by the Bonferroni post hoc analysis for multiple comparisons.

FOR SCURRY BROOKS ONLY

and *IL32* (Figure S6). For example, *LPHN2* (latrophilin 2) receptor, also known as *ADGRL2*, was downregulated in response to ImP stimulation. This gene is linked to angiogenic and neurotrophic effects in ECs and mouse tissue explants through deglycosylated LRG1 (leucine-rich-2-glycoprotein 1)/LPHN2 complex.[27] Other proangiogenic genes downregulated by ImP were calcitonin receptor-like (*CALCRL*), a G-protein–coupled receptor,[28] vascular endothelial growth factor receptor 1 (*FLT1*),[28,29] and transmembrane 4 L 6 family 18 (*TM4SF18*),[29] which are known to promote endothelial migration and proliferation in vitro. The expression of 2 genes involved in heart development and morphogenesis regulating EC migration was also decreased by ImP: *DCHS1*, a member of the cadherin superfamily,[30] and *FLRT2*, a member of the fibronectin leucine-rich transmembrane family. In contrast, the expression of angiogenesis-inhibitory genes, including angiopoietin-like 4 (*ANGPTL4*),[31] a Rac-specific GTPase isoform of *ARHGAP22* (p68RacGAP)[32] and interleukin 32 (*IL-32*),[33] was upregulated by ImP. Thus, the gene expression pattern may provide insights into the underlying mechanisms responsible for the consistent reduction in endothelial wound healing capacity observed after ImP treatment.

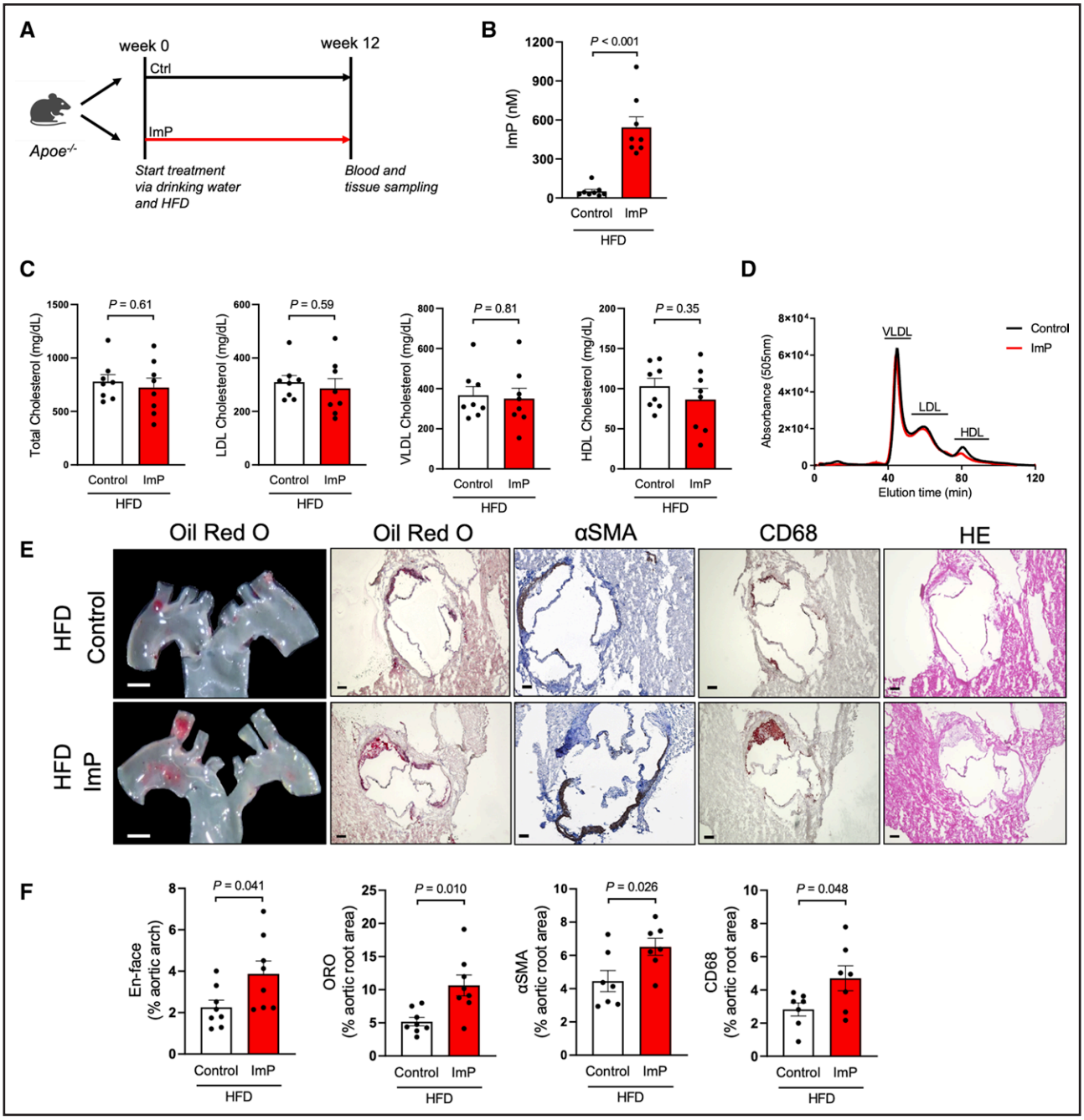

Figure 4. Imidazole propionate (ImP) aggravates high-fat diet (HFD)–induced atherosclerosis in *Apoe*$^{-/-}$ mice.
A, Schematic illustration of the mouse model of atherosclerosis. *Apoe*$^{-/-}$ mice were fed a HFD and treated with and without ImP (800 μg/d) in drinking water for 12 weeks (n=8). **B**, Plasma levels of ImP in *Apoe*$^{-/-}$ mice after 12-week treatment of HFD and exposure to drinking water or ImP (800 μg/d). **C**, Evaluation of levels of total cholesterol (TC), VLDL (very-low-density lipoprotein), LDL (low-density lipoprotein) cholesterol, and HDL (high-density lipoprotein) cholesterol in fasting plasma of control mice or ImP-treated mice fed an HFD. **D**, Ultra-high performance liquid chromatography (UHPLC)–derived lipoprotein fractions in plasma from control vs ImP mice fed an HFD. Lipoproteins were detected by absorbance at 505 nm and at different elution times. **E**, Representative images of oil red O (ORO)–stained en face aortic arch and of aortic root sections stained with ORO, αSMA (α-smooth muscle actin), CD68, and hematoxylin/eosin (HE; scale bars represent 1 mm for en face images or 100 μm for aortic root images). **F**, Quantification of atherosclerotic plaque area in en face aortic arch and total aortic root area, as well as of αSMA and CD68 of control vs ImP-treated mice as percentages. Data are shown as mean±SEM and were calculated by 2-tailed Mann-Whitney *U* test (**B**) or unpaired 2-tailed Student *t* test (**C** and **F**; n=8 per group). Unequal variance analysis in data (**F**, ORO staining of the aortic root) was assessed by the Welch *t* test.

Moreover, we found reduced expression of *PIK3C2A*, which encodes phosphatidylinositol-4-phosphate 3-kinase catalytic subunit type 2 (Figure 5C), an enzyme that belongs to the PI3K (phosphoinositide 3-kinase) family,[34] which is known to be activated upon insulin receptor stimulation.[35] Western blot analysis confirmed

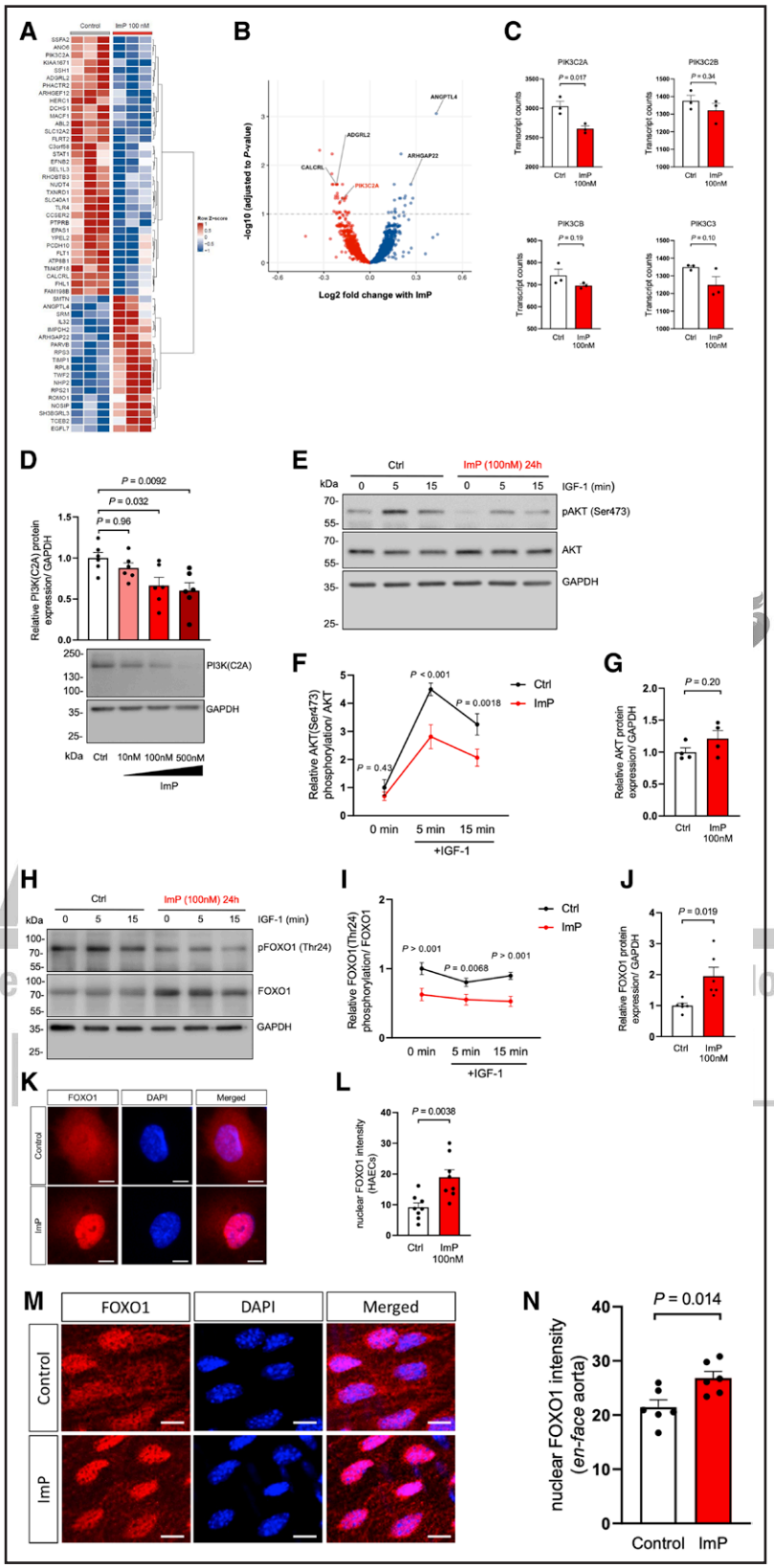

Figure 5. Imidazole propionate (ImP) suppresses PI3K (phosphoinositide 3-kinase)/AKT signaling and promotes nuclear translocation of FOXO1 (forkhead box O transcription factor) in endothelial cells.

RNA-sequencing analysis of human aortic endothelial cells (HAECs). **A**, Heatmap with 52 differentially expressed genes between ImP and control conditions (adjusted $P<0.1$). Read counts were transformed to Z scores (ie, zero mean, unit variance scaling). The dendrogram on the right was drawn using hierarchical clustering (Ward method). **B**, Volcano plot. Red dots represent genes with lower expression (*Continued*)

reduced expression of PI3K-C2A at the protein level (Figure 5D). To further explore whether ImP modulates signaling pathways linked to PI3K, we pretreated ECs with ImP for 24 hours followed by insulin receptor activation with IGF-1 stimulation. We observed that ImP reduced AKT phosphorylation (at the activation site of Ser473; Figure 5E through 5G) and increased FOXO1 activation. Since the FOXOs are established effectors of the PI3K/AKT pathway and essential regulators of EC growth,[36] we sought to examine whether dysregulation of FOXO family members links ImP-induced suppression of the PI3K/AKT pathway with impaired angiogenic activity in ECs. FOXO1 is the predominant FOXO family member in ECs.[37] Activation of the PI3K pathway, for example, upon insulin receptor stimulation, inhibits FOXO1 through AKT-dependent phosphorylation, resulting in DNA-binding inhibition, FOXO1 nuclear exclusion, and subsequent cytoplasmic sequestration.[37] Nuclear exclusion of FOXO1 leads to the activation of a number of angiogenesis-promoting genes in ECs, thereby promoting endothelial angiogenic activity.[36] In this study, ImP decreased phosphorylation of FOXO1 at AKT-dependent site (Figure 5H through 5J) and led to FOXO1 nuclear translocation both in vitro (Figure 5K and 5L) and in vivo (Figure 5M and 5N).

SiRNA-mediated FOXO1 knockdown abolished the ImP-induced increase in ICAM-1 and VCAM-1 levels compared with control HAECs (Figure 6A and 6B). Consistent with these observations, we found improved vascular regeneration after carotid injury in ImP-treated EC-specific *FOXO1* knockout mice (*Cdh5-CreERT2*$^{(+/-)}$/*FOXO1*$^{fl/fl}$) compared with control littermates without Cre recombinase activity (*Cdh5-CreERT2*$^{(+/+)}$/*FOXO1*$^{fl/fl}$; Figure 6C through 6E). Together, these findings support the involvement of a FOXO1-dependent pathway in ImP signaling leading to reduced vascular regeneration and a proinflammatory response.

DISCUSSION

Our study demonstrates that elevated plasma levels of the gut microbial metabolite ImP are associated with increased prevalence of CAD in humans even after adjusting for traditional cardiovascular risk factors. Furthermore, we provide evidence that ImP causally contributes to the development of atherosclerosis by impairing EC functions in both in vitro and in vivo models.

Mechanistically, we identified that ImP disrupts endothelial PI3K/AKT signaling and activates the nuclear FOXO1 transcription factor, thereby restricting the proliferative and migratory activities of ECs. This impairment leads to a reduced capacity for endothelial regeneration following arterial injury in vivo. Ultimately, these effects of ImP accelerate the progression of atherosclerosis, thereby linking it to the pathophysiology of ACVD (Graphic Abstract).

Accelerated vascular disease is a major determinant of increased morbidity and mortality risk in patients with diabetes,[38] and injury to the arterial wall is considered a crucial step for the onset and progression of atherosclerotic vascular disease.[1] Endothelial denudation upon arterial wall injury induces a cascade of cellular and molecular actions, ultimately leading to vascular wall remodeling, which initiates or promotes the development of atherosclerotic vascular disease.[39] This process includes leukocyte chemotaxis with secretion of an array of cytokines and growth factors that govern the migration and proliferation of smooth muscle cells and interstitial collagen gene expression, leading to extracellular matrix deposition following injury.[40] While proper EC repair may mitigate pathological alterations of the vascular wall by stabilizing vulnerable plaques, impaired regenerative capacity of the endothelium facilitates adverse vascular wall remodeling, thereby promoting atherosclerosis.[41,42]

A dysfunctional endothelium often emerges in lesion-prone regions of the arterial vasculature and induces early atherosclerotic changes.[1] This dysfunction is characterized

ATVB Arteriosclerosis, Thrombosis, and Vascular Biology FIRST PROOF ONLY

Figure 5 Continued. in ImP-treated HAECs compared with control group, while blue dots represent genes with higher expression. *x* axis denotes the log2-fold change values, and the *y* axis shows the −log10 adjusted *P* values. **C**, Transcript counts from genes of PI3K (phosphoinositide 3-kinase) family of different isoforms including *PIK3C2A*, *PIK3C2B*, *PIK3CB*, and *PIK3C3*. Quantitative data are from 3 independent experiments (n=3). **D**, Dose-dependent quantification of PI3K(C2A) protein levels in endothelial cells stimulated with control medium, 10 nmol/L ImP, 100 nmol/L ImP, or 500 nmol/L ImP. Below are representative Western blots of PI3K(C2A) expression normalized to GAPDH (n=6 per group). **E**, Endothelial cells were treated with 100 nmol/L ImP for 24 hours followed by IGF-1 stimulation for 0, 5, and 15 minutes. Representative Western blots show protein levels of phospho-AKT(Ser473), AKT, and GAPDH (n=4 per group). **F**, Time-dependent quantification of relative AKT(Ser473) phosphorylation normalized to total AKT protein expression. **G**, Quantification of relative total AKT protein levels normalized to GAPDH expression. **H**, Representative Western blots illustrate the protein expression of phospho-FOXO1(Thr24), FOXO1, and GAPDH expression (n=6 per group). **I**, Time-dependent quantification of relative FOXO1(Thr24) phosphorylation normalized to total FOXO1 protein expression. **J**, Quantification of relative FOXO1 protein level normalized to GAPDH expression. **K**, Immunostaining of human aortic endothelial cells showing nuclear sublocalization of FOXO1 (red) and DAPI (4′,6-diamidino-2-phenylindole)-stained nucleus (blue; ×40 magnification; scale bars represent 10 μm). **L**, Quantification of nuclear FOXO1 intensity between control and 100 nmol/L ImP (n=8 per group). **M**, FOXO1 (red) en face immunostaining of aorta from mice treated with and without ImP via drinking water. Nuclei were counterstained by DAPI (blue; ×40 oil immersion magnification; scale bars represent 50 μm). **N**, Quantification of nuclear FOXO1 intensity in the aorta of control and ImP groups (n=6). Data are shown as mean±SEM and were calculated by 1-way ANOVA followed by the Bonferroni post hoc analysis (**D**), 2-way ANOVA followed by the Bonferroni post hoc analysis for multiple comparisons between control and ImP at different time points (**F** and **I**, independent experiments of n=6), or unpaired 2-tailed Student *t* test between 2 groups (**C**, **G**, **J**, **L**, and **N**). Unequal variance analysis in data (**J**) was assessed by the Welch *t* test.

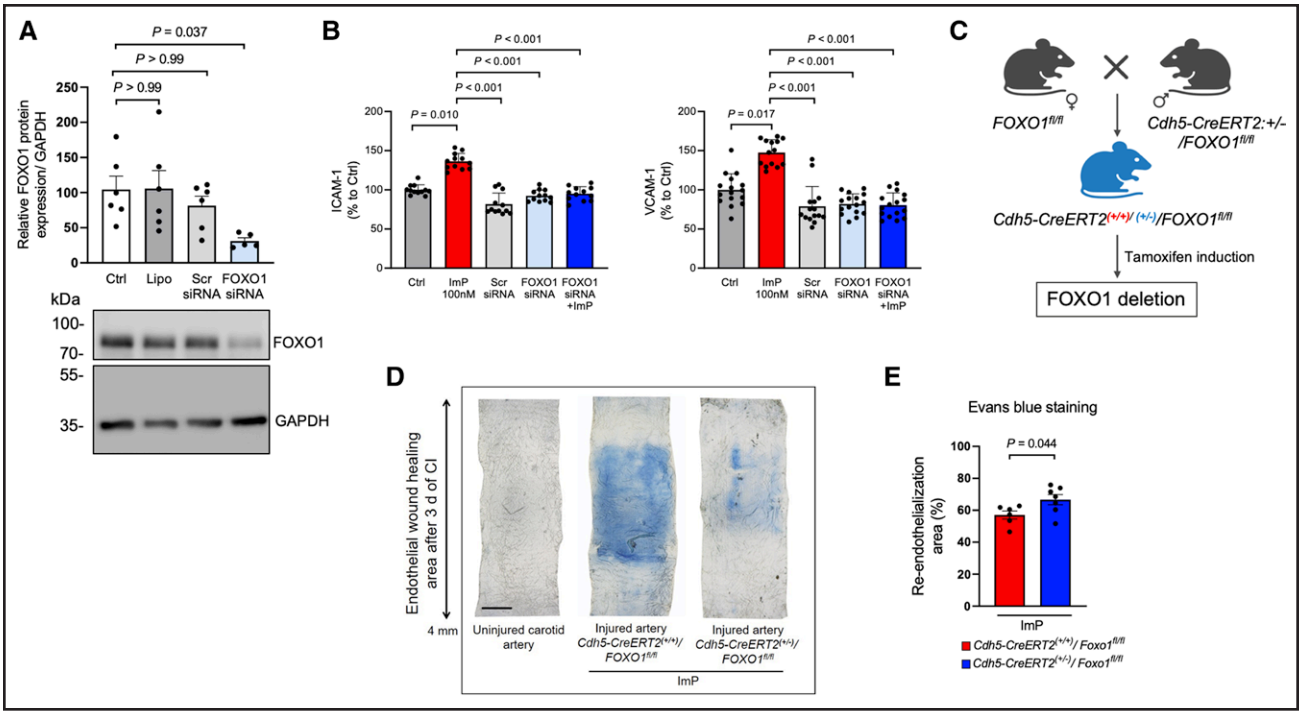

Figure 6. Inhibition of endothelial-specific FOXO1 (forkhead box O transcription factor-1) restores imidazole propionate (ImP)-mediated effects on endothelial inflammation and vascular damage.
A, Quantification of FOXO1 knockdown in endothelial cells on protein levels. Below are the representative Western blots of FOXO1 protein levels after 4 hours of small interfering RNA (siRNA) transfection. Total FOXO1 protein expression was normalized to GAPDH expression (n=5 for the FOXO1 siRNA group and n=6 for all other groups). **B**, Flow cytometric analysis representing data of cellular adhesion surface expression of ICAM-1 (intercellular adhesion molecule-1; n=12) and VCAM-1 (vascular cell adhesion molecule-1; n=16) in FOXO1-silenced human aortic endothelial cells (HAECs) followed by ImP treatment for 24 hours. Control groups include control medium, scramble (Scr) siRNA, and FOXO1 siRNA. **C**, Schematic illustration of endothelial-specific FOXO1 knockout mice using tamoxifen-inducible Cre-loxP system. *LoxP*-flanked FOXO1 mice (*FOXO1*$^{fl/fl}$) were crossbred with transgenic mice expressing the tamoxifen-inducible vascular endothelial-specific cadherin (*Cdh5*) promoter-driven CreERT2 recombinase (*Cdh5-CreERT2:+/–*). Deletion of FOXO1 in endothelial cells was induced in the presence of Cre recombinase through intraperitoneal injections of tamoxifen (100 mg/kg per body weight) once a day for 5 consecutive days. FOXO1 knockout mice are referred to as *Cdh5-CreERT2*$^{(+/-)}$*/FOXO1*$^{fl/fl}$, while control animals were littermates without Cre recombinase activity and are referred to as *Cdh5-CreERT2*$^{(+/+)}$*/FOXO1*$^{fl/fl}$. **D**, Representative en face images of Evans blue–stained carotid arteries: uninjured carotid artery, and injured carotid artery from control littermates (*Cdh5-CreERT2*$^{(+/+)}$*/FOXO1*$^{fl/fl}$) and from FOXO1 deficiency mice (*Cdh5-CreERT2*$^{(+/-)}$*/FOXO1*$^{fl/fl}$). The blue-stained area corresponds to the denuded area of injured carotid arteries (×5 magnification; scale bar represents 500 μm). **E**, Quantification of reendothelialization as the ratio of blue-stained area to total injured area in percentage (n=6 per group). Data are shown as mean±SEM and were calculated by 1-way ANOVA followed by the Bonferroni post hoc analysis (**A**), Kruskal-Wallis test followed by the Dunn post hoc analysis for multiple (**B**) or unpaired 2-tailed Student *t* test between control littermates without Cre recombinase activity, and FOXO1 deficiency animals upon ImP treatment (**E**).

AHA Arteriosclerosis, Thrombosis, and Vascular Biology FIRST PROOF ONLY

by an impairment of fundamental cellular properties such as migration and proliferation, which are essential for vascular repair.[43] Additionally, a dysfunctional endothelium is associated with increased vascular inflammation and matrix degradation, which contribute to plaque vulnerability and the risk of rupture, thereby promoting acute atherothrombotic events.[1,44] Despite enormous efforts to elucidate the mechanisms of EC dysfunction over the past decades, contributing pathways at the systems level are not fully understood. One hypothesis is that defective insulin receptor signaling, for example, due to impaired glucose tolerance or diabetes,[3] is a major cause of EC dysfunction, compromising the regenerative potential and being associated with a substantially increased risk of ACVD.[45]

In recent years, increasing evidence has demonstrated that alterations of the gut microbiota, its metabolic capacities, intestinal gene expression, and intestinal immune system are important contributing factors to cardiometabolic diseases,[13–15,46] which may contribute to endothelial dysfunction and ACVD.[47] The altered microbiota associated with cardiometabolic diseases can produce disease-causing and disease-modifying metabolites.[48] For instance, trimethylamine *N*-oxide, a metabolite produced by gut microbial metabolism of trimethylamine-rich nutrients like choline and carnitine, has been shown to promote atherosclerosis in animal models[5] and is associated with poorer prognosis in patients with coronary heart disease, chronic kidney disease, and ischemic stroke.[10] The gut microbiota-dependent trimethylamine *N*-oxide pathway contributes to both development of renal insufficiency and mortality risk in chronic kidney disease.[12,49] Conversely, short-chain

fatty acids, such as acetic, propionic, and butyric acids, produced through microbial fermentation of dietary fibers have demonstrated positive effects on host metabolism and cardiovascular health.[50,51]

The microbially produced, histidine-derived metabolite ImP is increased in the portal and peripheral blood of patients with obesity and type 2 diabetes compared with controls.[17] These findings were confirmed in patients of different geographic location, and ImP was found to be associated with low bacterial gene richness.[18] Recently, ImP was found to be increased in patients with heart failure.[20] However, it is unknown how ImP affects EC function and ACVD. Our findings demonstrate a link between ImP levels and increased risk for prevalent CAD in humans, and we provide evidence of potential causality using chronic administration of ImP to atherosclerosis prone chronic administration of ImP to atherosclerosis prone mice in a lipid-independent mechanism.

Our studies indicate that ImP exerts deleterious effects on ECs, resulting in a reduced regenerative capability of the endothelium after vascular injury. Specifically, we show that ImP impairs the ability of ECs to activate insulin receptor–induced PI3K/AKT signaling by downregulating PI3K-C2A. This disruption in PI3K/AKT signaling is accompanied by decreased phosphorylation and increased nuclear accumulation of FOXO1, which may underlie the weakened repair capacity of the endothelium. These findings are consistent with previous reports showing that FOXO1 plays a pivotal role in endothelial function by linking metabolic activity, including glycolysis and mitochondrial respiration, to cellular growth states.[36] Notably, FOXO1 deficiency in ECs appears to counteract the harmful effects of ImP on EC function, thereby enhancing vascular repair mechanisms.

Taken together, these findings offer a rationale for developing novel preventive strategies aimed at reducing gut microbial production of ImP. One such approach could involve specifically inhibiting the enzymatic activity of UrdA (urocanate reductase), which converts urocanate, a metabolite of L-histidine, into ImP. In this context, previously reported high-resolution structures of UrdA provide critical insights into the conformational changes associated with substrate and product binding, paving the way for future interventions targeting the enzyme's active site to modulate microbial ImP production.[52]

In conclusion, our findings demonstrate a link between ImP and EC dysfunction, which involves a deregulated PI3K/AKT/FOXO1 signaling axis. Moreover, they demonstrate a causal role of ImP in the development of ACVD and thus suggest therapeutic effects of targeting ImP-producing gut microbial pathways in cardiovascular disease prevention.

ARTICLE INFORMATION

Received December 18, 2024; accepted March 5, 2025.

Affiliations

Department of Cardiology, Angiology and Intensive Care Medicine, Deutsches Herzzentrum der Charité, Campus Benjamin Franklin, Berlin, Germany (V.N., L.R., J.S., P.R.R., E.T.S., N.K., U.L., A.H.). German Center for Cardiovascular Research (DZHK), Partner Site Berlin, Germany (V.N., L.R., P.R.R., L.P., E.T.S., N.K., M.P., W.M.K., U.L., A.H.). Friede Springe-Cardiovascular Prevention Center at Charité, Charité-Universitätsmedizin Berlin, Germany (V.N., J.S., E.S.-T., N.K., U.L., A.H.). Institute of Chemistry and Biochemistry, Freie Universität Berlin, Germany (V.N., P.K.). University Hospital St. Josef-Hospital Bochum, Cardiology and Rhythmology, Ruhr University Bochum, Germany (V.N., L.R., A.H.). Department of Molecular and Clinical Medicine, Wallenberg Laboratory, Sahlgrenska University Hospital, University of Gothenburg, Sweden (A.C., K.R.B., M.H., F.B.). Berlin Institute of Health at Charité-Universitätsmedizin Berlin, Germany (J.S., U.L., A.H.). Institute of Physiology, Charité-Universitätsmedizin Berlin, corporate member of the Freie Universität Berlin and Humboldt-Universität zu Berlin, Germany (L.P., W.M.K.). Institute of Biology, Freie Universität Berlin, Germany (L.P.). Angiogenesis and Metabolism Laboratory, Berlin Institute of Health at Charité-Universitätsmedizin Berlin, Germany (J.L., M.P.). Max Delbrück Center for Molecular Medicine in the Helmholtz Association, Berlin, Germany (J.L., M.P.). Department of Internal Medicine-Geriatrics, Amsterdam Cardiovascular Sciences, Amsterdam University Medical Center (UMC), the Netherlands (B.V., M.N.). Department of Vascular Medicine, Amsterdam UMC, the Netherlands (B.V., M.N.). Institute for Cardiovascular Prevention (IPEK), Ludwig Maximilian University of Munich, Germany (Y.D., C.W.). Division of Angiology, Swiss Cardiovascular Center, Inselspital, Bern University Hospital (Y.D.) and Department for BioMedical Research, University of Bern (Y.D.), Switzerland. German Center for Cardiovascular Research (DZHK), Partner Site Munich, Germany (Y.D., C.W.). Department of Biochemistry, Cardiovascular Research Institute Maastricht, Maastricht University Medical Centre, the Netherlands (C.W.). Munich Cluster for Systems Neurology, Germany (C.W.). Department of Internal Medicine D–Geriatrics, University Medicine Greifswald, Germany (M.K.). Department of Endocrinology and Metabolic Diseases (including Division of Lipid Metabolism), Charité-Universitätsmedizin Berlin, corporate member of the Freie Universität Berlin and Humboldt-Universität zu Berlin, Germany (E.S.-T., I.D.). Charité–Universitätsmedizin Berlin, Berlin Institute of Health Center for Regenerative Therapies, Germany (I.D.). German Center for Cardiovascular Research (DZHK), Partner Site Frankfurt Rhine-Main, Germany (D.M.L.). Department of Medicine, Cardiology and Angiology, Goethe University Hospital, Frankfurt, Germany (D.M.L.). Berlin-Brandenburg School for Regenerative Therapies, Germany (P.K.). International Max-Planck Research School for Biology and Computation, Berlin, Germany (P.K.). German Center for Lung Research (DZL), Berlin, Germany (W.M.K.). Keenan Research Centre for Biomedical Science at St. Michael's, Toronto, Canada (W.M.K.). Departments of Surgery and Physiology, University of Toronto, Canada (W.M.K.). Departments of Cardiovascular and Metabolic Sciences, and Cardiovascular Medicine, Cleveland Clinic, OH (M.F., I.N., S.L.H.). Department of Molecular Medicine, Cleveland Clinic Lerner College of Medicine of Case Western Reserve University School of Medicine, OH (S.L.H.). Department of Clinical Physiology, Region Västra Götaland, Sahlgrenska University Hospital, Gothenburg, Sweden (F.B.).

Acknowledgments

The authors thank M. Moobed and N. Rösener for excellent assistance on cell culture experiments and Y. Jansen and S. Bayasgalan on performing lipid profiling in mice. V. Nageswaran designed and performed the in vitro and in vivo experiments and contributed to the bioinformatic data analysis. A. Carreras, K.R. Beck, I. Nemet, M.S., and F. Bäckhed designed the imidazole propionate drinking protocol and performed mass spectrometry analysis in human and mouse samples. I. Demuth, U. Landmesser, and E. Steinhagen-Thiessen are the PIs of the LipidCardio study and contributed data and clinical samples. M. König (LipidCardio study physician), D.M. Leistner, and A. Haghikia were involved in baseline and follow-up LipidCardio data acquisition. J. Steinfeldt contributed to the bioinformatic data analysis of the human study. L. Reinshagen, P. Ramezani Rad, E.T. Strässler, and N. Kränkel provided general experimental support. L. Peters conducted wire myography in mice. B. Verhaar performed RNA-sequencing bioinformatics analysis. Y. Döring and C. Weber performed the lipid analysis. J. Lim and M. Potente provided endothelial-specific FOXO1 (forkhead box O transcription factor-1) knockout animals and supported experimental work. M. Nieuwdorp, P. Knaus, W.M. Kuebler, and E. Steinhagen-Thiessen supported the research and provided valuable input. M. Ferrell and S.L. Hazen performed the mass spectrometry analysis in human samples and ELISA of soluble VCAM-1 (vascular cell adhesion molecule-1). A. Haghikia, F. Bäckhed, and U. Landmesser supervised the project. V. Nageswaran and A. Haghikia wrote the paper. All authors reviewed and approved the manuscript.

Sources of Funding

This study was funded by the Transatlantic Networks of Excellence Award from the Leducq Foundation (17CVD01), Sympath (Systems Medicine of

Arteriosclerosis, Thrombosis, and Vascular Biology
FIRST PROOF ONLY

Pneumonia-Aggravated Atherosclerosis; grant number 01ZX1906B), the German Federal Ministry of Education and Research (BMBF), and by grants from the German Heart Research Foundation (DSHF F/01/22), German Center for Cardiovascular Research (DZHK; rotation grant), the Else Kröner-Fresenius-Stiftung (2017_A100), and the German Research Foundation (DFG; HA 6951/2-1) to A. Haghikia and the Swedish Heart Lung Foundation (20210366) to F. Bäckhed. F. Bäckhed is Torsten Söderberg Professor in Medicine and Wallenberg Scholar, and A. Haghikia was a participant in the Berlin Institute of Health (BIH)–Charité Advanced Clinician Scientist Pilot Program funded by the Charité Universitätsmedizin Berlin and the BIH. M. Nieuwdorp is supported by a personal ZONMW-VICI grant 2020 (09150182010020). S.L. Hazen notes laboratory support by the National Institutes of Health (NIH) grant P01 HL147823 and NIH and Office of Dietary Supplements grant R01HL103866. The LipidCardio Study was partially funded by Sanofi-Aventis Deutschland GmbH (I. Demuth and E. Steinhagen-Thiessen).

Disclosures

F. Bäckhed, A. Carreras, and K.R. Beck, are cofounders and shareholders of Implexion Pharma AB. F. Bäckhed is the cofounder of Roxbiosens Inc, receives research funding from Biogaia AB and Novo Nordisk A/s, and is a member of the scientific advisory board of Bactolife A/s. M. Nieuwdorp is the cofounder and shareholder of Caelus Health. S.L. Hazen reports being named as the coinventor on pending and issued patents held by the Cleveland Clinic relating to cardiovascular diagnostics and therapeutics, being a paid consultant formerly for Procter & Gamble, and currently being with Zehna Therapeutics, having received research funds from Procter & Gamble, Zehna Therapeutics, and Roche Diagnostics, and being eligible to receive royalty payments for inventions or discoveries related to cardiovascular diagnostics or therapeutics from Procter & Gamble, Zehna Therapeutics, and Cleveland HeartLab, a wholly owned subsidiary of Quest Diagnostics. The other authors report no conflicts.

Supplemental Material

Figures S1–S6
Major Resources Table
Unedited Gels

REFERENCES

1. Gimbrone MA Jr, García-Cardeña G. Endothelial cell dysfunction and the pathobiology of atherosclerosis. *Circ Res*. 2016;118:620–636. doi: 10.1161/CIRCRESAHA.115.306301
2. Silvestre-Roig C, Braster Q, Ortega-Gomez A, Soehnlein O. Neutrophils as regulators of cardiovascular inflammation. *Nat Rev Cardiol*. 2020;17:327–340. doi: 10.1038/s41569-019-0326-7
3. Eelen G, de Zeeuw P, Simons M, Carmeliet P. Endothelial cell metabolism in normal and diseased vasculature. *Circ Res*. 2015;116:1231–1244. doi: 10.1161/CIRCRESAHA.116.302855
4. Wu J, Wang K, Wang X, Pang Y, Jiang C. The role of the gut microbiome and its metabolites in metabolic diseases. *Protein Cell*. 2021;12:360–373. doi: 10.1007/s13238-020-00814-7
5. Koeth RA, Wang Z, Levison BS, Buffa JA, Org E, Sheehy BT, Britt EB, Fu X, Wu Y, Li L, et al. Intestinal microbiota metabolism of L-carnitine, a nutrient in red meat, promotes atherosclerosis. *Nat Med*. 2013;19:576–585. doi: 10.1038/nm.3145
6. Wang Z, Roberts AB, Buffa JA, Levison BS, Zhu W, Org E, Gu X, Huang Y, Zamanian-Daryoush M, Culley MK, et al. Non-lethal inhibition of gut microbial trimethylamine production for the treatment of atherosclerosis. *Cell*. 2015;163:1585–1595. doi: 10.1016/j.cell.2015.11.055
7. Witkowski M, Witkowski M, Friebel J, Buffa JA, Li XS, Wang Z, Sangwan N, Li L, DiDonato JA, Tizian C, et al. Vascular endothelial tissue factor contributes to trimethylamine N-oxide-enhanced arterial thrombosis. *Cardiovasc Res*. 2022;118:2367–2384. doi: 10.1093/cvr/cvab263
8. Jäckel S, Kiouptsi K, Lillich M, Hendrikx T, Khandagale A, Kollar B, Hörmann N, Reiss C, Subramaniam S, Wilms E, et al. Gut microbiota regulate hepatic von Willebrand Factor synthesis and arterial thrombus formation via Toll-like receptor-2. *Blood*. 2017;130:542–553. doi: 10.1182/blood-2016-11-754416
9. Kiouptsi K, Jäckel S, Pontarollo G, Grill A, Kuijpers MJE, Wilms E, Weber C, Sommer F, Nagy M, Neideck C, et al. The microbiota promotes arterial thrombosis in low-density lipoprotein receptor-deficient mice. *mBio*. 2019;10:e02298–e02219. doi: 10.1128/mBio.02298-19
10. Tang WHW, Wang Z, Levison BS, Koeth RA, Britt EB, Fu X, Wu Y, Hazen SL. Intestinal microbial metabolism of phosphatidylcholine and cardiovascular risk. *N Engl J Med*. 2013;368:1575–1584. doi: 10.1056/NEJMoa1109400
11. Wang M, Li XS, Wang Z, de Oliveira O, Marcia C, Lemaitre RN, Fretts A, Sotoodehnia N, Budoff M, Nemet I, et al. Trimethylamine N-oxide is associated with long-term mortality risk: the multi-ethnic study of atherosclerosis. *Eur Heart J*. 2023;44:1608. doi: 10.1093/eurheartj/ehad089
12. Haghikia A, Li XS, Liman TG, Bledau N, Schmidt D, Zimmermann F, Kränkel N, Widera C, Sonnenschein K, Haghikia A, et al. Gut microbiota-dependent trimethylamine N-oxide predicts risk of cardiovascular events in patients with stroke and is related to proinflammatory monocytes. *Arterioscler Thromb Vasc Biol*. 2018;38:2225–2235. doi: 10.1161/ATVBAHA.118.311023
13. Qin J, Li Y, Cai Z, Li S, Zhu J, Zhang F, Liang S, Zhang W, Guan Y, Shen D, et al. A metagenome-wide association study of gut microbiota in type 2 diabetes. *Nature*. 2012;490:55–60. doi: 10.1038/nature11450
14. Wu H, Tremaroli V, Schmidt C, Lundqvist A, Olsson LM, Krämer M, Gummesson A, Perkins R, Bergström G, Bäckhed F. The gut microbiota in prediabetes and diabetes: a population-based cross-sectional study. *Cell Metab*. 2020;32:379–390.e3. doi: 10.1016/j.cmet.2020.06.011
15. Karlsson FH, Tremaroli V, Nookaew I, Bergström G, Behre CJ, Fagerberg B, Nielsen J, Bäckhed F. Gut metagenome in European women with normal, impaired and diabetic glucose control. *Nature*. 2013;498:99–103. doi: 10.1038/nature12198
16. Wilmanski T, Rappaport N, Earls JC, Magis AT, Manor O, Lovejoy J, Omenn GS, Hood L, Gibbons SM, Price ND. Blood metabolome predicts gut microbiome α-diversity in humans. *Nat Biotechnol*. 2019;37:1217–1228. doi: 10.1038/s41587-019-0233-9
17. Koh A, Molinaro A, Ståhlman M, Khan MT, Schmidt C, Mannerås-Holm L, Wu H, Carreras A, Jeong H, Olofsson LE, et al. Microbially produced imidazole propionate impairs insulin signaling through mTORC1. *Cell*. 2018;175:947–961.e17. doi: 10.1016/j.cell.2018.09.055
18. Molinaro A, Bel Lassen P, Henricsson M, Wu H, Adriouch S, Belda E, Chakaroun R, Nielsen T, Bergh P-O, Rouault C, et al; MetaCardis Consortium. Imidazole propionate is increased in diabetes and associated with dietary patterns and altered microbial ecology. *Nat Commun*. 2020;11:5881. doi: 10.1038/s41467-020-19589-w
19. Koh A, Mannerås-Holm L, Yunn N-O, Nilsson PM, Ryu SH, Molinaro A, Perkins R, Smith JG, Bäckhed F. Microbial imidazole propionate affects responses to metformin through p38γ-dependent inhibitory AMPK phosphorylation. *Cell Metab*. 2020;32:643–653.e4. doi: 10.1016/j.cmet.2020.07.012
20. Molinaro A, Nemet I, Bel Lassen P, Chakaroun R, Nielsen T, Aron-Wisnewsky J, Bergh P-O, Li L, Henricsson M, Køber L, et al; MetaCardis Consortium. Microbially produced imidazole propionate is associated with heart failure and mortality. *JACC Heart Fail*. 2023;11:810–821. doi: 10.1016/j.jchf.2023.03.008
21. König M, Joshi S, Leistner DM, Landmesser U, Sinning D, Steinhagen-Thiessen E, Demuth I. Cohort profile: role of lipoproteins in cardiovascular disease-the LipidCardio study. *BMJ Open*. 2019;9:e030097. doi: 10.1136/bmjopen-2019-030097
22. Andrade J, Shi C, Costa ASH, Choi J, Kim J, Doddaballapur A, Sugino T, Ong YT, Castro M, Zimmermann B, et al. Control of endothelial quiescence by FOXO-regulated metabolites. *Nat Cell Biol*. 2021;23:413–423. doi: 10.1038/s41556-021-00637-6
23. Sorrentino SA, Bahlmann FH, Besler C, Müller M, Schulz S, Kirchhoff N, Doerries C, Horváth T, Limbourg A, Limbourg F, et al. Oxidant stress impairs in vivo reendothelialization capacity of endothelial progenitor cells from patients with type 2 diabetes mellitus: restoration by the peroxisome proliferator-activated receptor-gamma agonist rosiglitazone. *Circulation*. 2007;116:163–173. doi: 10.1161/CIRCULATIONAHA.106.684381
24. Okabe K, Kobayashi S, Yamada T, Kurihara T, Tai-Nagara I, Miyamoto T, Mukouyama Y, Sato TN, Suda T, Ema M, et al. Neurons limit angiogenesis by titrating VEGF in retina. *Cell*. 2014;159:584–596. doi: 10.1016/j.cell.2014.09.025
25. Anders S, Huber W. Differential expression analysis for sequence count data. *Genome Biol*. 2010;11:R106. doi: 10.1186/gb-2010-11-10-r106
26. Videm V, Albrigtsen M. Soluble ICAM-1 and VCAM-1 as markers of endothelial activation. *Scand J Immunol*. 2008;67:523–531. doi: 10.1111/j.1365-3083.2008.02029.x
27. Yin GN, Kim D-K, Kang JI, Im Y, Lee DS, Han A-R, Ock J, Choi M-J, Kwon M-H, Limanjaya A, et al. Latrophilin-2 is a novel receptor of LRG1 that rescues vascular and neurological abnormalities and restores diabetic erectile function. *Exp Mol Med*. 2022;54:626–638. doi: 10.1038/s12276-022-00773-5
28. Tuo Y, Guo X, Zhang X, Wang Z, Zhou J, Xia L, Zhang Y, Wen J, Jin D. The biological effects and mechanisms of calcitonin gene-related peptide on human endothelial cell. *J Recept Signal Transduct Res*. 2013;33:114–123. doi: 10.3109/10799893.2013.770528

American Heart Association.
ATVB Arteriosclerosis, Thrombosis, and Vascular Biology
FIRST PROOF ONLY

29. Page DJ, Thuret R, Venkatraman L, Takahashi T, Bentley K, Herbert SP. Positive feedback defines the timing, magnitude, and robustness of angiogenesis. *Cell Rep*. 2019;27:3139–3151.e5. doi: 10.1016/j.celrep.2019.05.052
30. Durst R, Sauls K, Peal DS, deVlaming A, Toomer K, Leyne M, Salani M, Talkowski ME, Brand H, Perrocheau M, et al. Mutations in DCHS1 cause mitral valve prolapse. *Nature*. 2015;525:109–113. doi: 10.1038/nature14670
31. Lamalice L, Le Boeuf F, Huot J. Endothelial cell migration during angiogenesis. *Circ Res*. 2007;100:782–794. doi: 10.1161/01.RES.0000259593.07661.1e
32. Aitsebaomo J, Wennerberg K, Der CJ, Zhang C, Kedar V, Moser M, Kingsley-Kallesen ML, Zeng G-Q, Patterson C. p68RacGAP is a novel GTPase-activating protein that interacts with vascular endothelial zinc finger-1 and modulates endothelial cell capillary formation. *J Biol Chem*. 2004;279:17963–17972. doi: 10.1074/jbc.M311721200
33. Meyer N, Akdis CA. Vascular endothelial growth factor as a key inducer of angiogenesis in the asthmatic airways. *Curr Allergy Asthma Rep*. 2013;13:1–9. doi: 10.1007/s11882-012-0317-9
34. Heng EYZ, Maffucci T. An overview of class II phosphoinositide 3-kinases. *Curr Top Microbiol Immunol*. 2022;436:51–68. doi: 10.1007/978-3-031-06566-8_2
35. Tsai S, Clemente-Casares X, Zhou AC, Lei H, Ahn JJ, Chan YT, Choi O, Luck H, Woo M, Dunn SE, et al. Insulin receptor-mediated stimulation boosts T cell immunity during inflammation and infection. *Cell Metab*. 2018;28:922–934.e4. doi: 10.1016/j.cmet.2018.08.003
36. Wilhelm K, Happel K, Eelen G, Schoors S, Oellerich MF, Lim R, Zimmermann B, Aspalter IM, Franco CA, Boettger T, et al. FOXO1 couples metabolic activity and growth state in the vascular endothelium. *Nature*. 2016;529:216–220. doi: 10.1038/nature16498
37. Potente M, Urbich C, Sasaki K, Hofmann WK, Heeschen C, Aicher A, Kollipara R, DePinho RA, Zeiher AM, Dimmeler S. Involvement of Foxo transcription factors in angiogenesis and postnatal neovascularization. *J Clin Invest*. 2005;115:2382–2392. doi: 10.1172/JCI23126
38. Nelson AJ, Peterson ED, Pagidipati NJ. Atherosclerotic cardiovascular disease and heart failure: determinants of risk and outcomes in patients with diabetes. *Prog Cardiovasc Dis*. 2019;62:306–314. doi: 10.1016/j.pcad.2019.07.001
39. La Sala L, Prattichizzo F, Ceriello A. The link between diabetes and atherosclerosis. *Eur J Prev Cardiol*. 2019;26:15–24. doi: 10.1177/2047487319878373
40. Weber C, Noels HA. Current pathogenesis and therapeutic options. *Nat Med*. 2011;17:1410–1422. doi: 10.1038/nm.2538
41. Schober A, Nazari-Jahantigh M, Wei Y, Bidzhekov K, Gremse F, Grommes J, Megens RTA, Heyll K, Noels H, Hristov M, et al. MicroRNA-126-5p promotes endothelial proliferation and limits atherosclerosis by suppressing Dlk1. *Nat Med*. 2014;20:368–376. doi: 10.1038/nm.3487
42. Döring Y, Noels H, van der V, Emiel PC, Neideck C, Egea V, Drechsler M, Mandl M, Pawig L, Jansen Y, et al. Vascular CXCR4 limits atherosclerosis by maintaining arterial integrity: evidence from mouse and human studies. *Circulation*. 2017;136:388–403. doi: 10.1161/CIRCULATIONAHA.117.027646
43. Michaelis UR. Mechanisms of endothelial cell migration. *Cell Mol Life Sci*. 2014;71:4131–4148. doi: 10.1007/s00018-014-1678-0
44. Wang L, Cheng CK, Yi M, Lui KO, Huang Y. Targeting endothelial dysfunction and inflammation. *J Mol Cell Cardiol*. 2022;168:58–67. doi: 10.1016/j.yjmcc.2022.04.011
45. Shah R, O'Neill SM, Hinkle C, Caughey J, Stephan S, Lynch E, Bermingham K, Lynch G, Ahima RS, Reilly MP. Metabolic effects of cx3cr1 deficiency in diet-induced obese mice. *PLoS One*. 2015;10:e0138317. doi: 10.1371/journal.pone.0138317
46. Karlsson FH, Fåk F, Nookaew I, Tremaroli V, Fagerberg B, Petranovic D, Bäckhed F, Nielsen J. Symptomatic atherosclerosis is associated with an altered gut metagenome. *Nat Commun*. 2012;3:1245. doi: 10.1038/ncomms2266
47. Catry E, Bindels LB, Tailleux A, Lestavel S, Neyrinck AM, Goossens J-F, Lobysheva I, Plovier H, Essaghir A, Demoulin J-B, et al. Targeting the gut microbiota with inulin-type fructans: preclinical demonstration of a novel approach in the management of endothelial dysfunction. *Gut*. 2018;67:271–283. doi: 10.1136/gutjnl-2016-313316
48. Chakaroun RM, Olsson LM, Bäckhed F. The potential of tailoring the gut microbiome to prevent and treat cardiometabolic disease. *Nat Rev Cardiol*. 2023;20:217–235. doi: 10.1038/s41569-022-00771-0
49. Tang WHW, Wang Z, Kennedy DJ, Wu Y, Buffa JA, Agatisa-Boyle B, Li XS, Levison BS, Hazen SL. Gut microbiota-dependent trimethylamine N-oxide (TMAO) pathway contributes to both development of renal insufficiency and mortality risk in chronic kidney disease. *Circ Res*. 2015;116:448–455. doi: 10.1161/CIRCRESAHA.116.305360
50. Koh A, Vadder F de, Kovatcheva-Datchary P, Bäckhed F. From dietary fiber to host physiology: short-chain fatty acids as key bacterial metabolites. *Cell*. 2016;165:1332–1345. doi: 10.1016/j.cell.2016.05.041
51. Haghikia A, Zimmermann F, Schumann P, Jasina A, Roessler J, Schmidt D, Heinze P, Kaisler J, Nageswaran V, Aigner A, et al. Propionate attenuates atherosclerosis by immune-dependent regulation of intestinal cholesterol metabolism. *Eur Heart J*. 2022;43:518–533. doi: 10.1093/eurheartj/ehab644
52. Venskutonytė R, Koh A, Stenström O, Khan MT, Lundqvist A, Akke M, Bäckhed F, Lindkvist-Petersson K. Structural characterization of the microbial enzyme urocanate reductase mediating imidazole propionate production. *Nat Commun*. 2021;12:1347. doi: 10.1038/s41467-021-21548-y

American Heart Association.
Arteriosclerosis, Thrombosis, and Vascular Biology
FIRST PROOF ONLY